Open Problems in Transport Physics of Ultrahigh-thermal Conductivity Materials

Xun Li and Li Shi<sup>a)</sup>

Walker Department of Mechanical Engineering and Texas Materials Institute

The University of Texas at Austin, Austin, Texas 78712, USA

<sup>a)</sup>Address all correspondence to this author. e-mail: lishi@mail.utexas.edu

Abstract

Recent searches of high-lattice thermal conductivity  $(\kappa_l)$  materials have explored size-

dependent non-diffusive phonon transport in low-dimensional systems and pursued compound

crystals with light and heavy elements. As a paradigm shift from past high- $\kappa_l$  criteria that

emphasize simple crystals made of light elements, the latter has led to ultrahigh- $\kappa_l$  semiconducting

boron arsenide (BAs) where a large phonon gap in such compounds limits three-phonon scattering

and makes four-phonon processes unusually important. Frequent four-phonon scattering and

consequently convergent  $\kappa_l$  have also been calculated in graphene because of numerous low-

frequency flexural phonons, raising a question whether high-order lattice anharmonicity is

sufficient to prevent graphene and carbon nanotubes from breaking the  $\kappa_l$  records of diamond and

graphite due to weakened phonon hydrodynamics. Open problems have also remained on four-

phonon processes in BAs, electron-phonon coupling effects in semiconductors and semimetals

including  $\theta$ -tantalum nitride with predicted high  $\kappa_l$ , and quantized lattice thermal conductance in

nanowires and nanotubes.

Keywords

Thermal conductivity; phonons; four-phonon scattering; electron-phonon coupling;

graphene; boron arsenide

1

#### Introduction

High-thermal conductivity ( $\kappa$ ) materials are in demand for addressing persistent technical challenges including thermal management of microelectronics [1] and for advancing emerging technologies such as electrification of industrial heating processes [2–4]. A clear understanding of the fundamental thermal transport mechanisms in solids is essential in the search of high- $\kappa$  materials for these various applications. Heat is conducted in solids by propagating thermal excitations of the lattice, electronic, and spin degrees of freedom. In general,  $\kappa$  is dominated by the electronic contribution ( $\kappa_e$ ) in metals and by the contribution ( $\kappa_l$ ) from phonons, the energy quanta of lattice vibrations, in semiconductors and dielectrics. Meanwhile, magnons and spinons, which are energy quanta of collective spin excitations with integer and fractional spins, respectively, can make an important contribution to  $\kappa$  in some metals and dielectrics with antiferromagnetic or ferromagnetic orders [5–9].

As shown in Figure 1, the currently accepted record-high  $\kappa$  values at room temperature are in the range between 2000 and 3000 Wm<sup>-1</sup>K<sup>-1</sup>, which are dominated by  $\kappa_l$  and measured respectively in high-quality crystals of semi-metallic graphite and ultrawide-bandgap diamond. As summarized by Slack into a set of criteria nearly half of a century ago [10], strong covalent bonding of the light carbon atoms in the relatively simple hexagonal and cubic crystal structures of graphite and diamond result in high phonon group velocities, few phonon polarizations, low phonon-phonon scattering rates, and thus high  $\kappa_l$ . Over the past two decades, a number of studies have investigated whether these records can be exceeded by exploiting the reduced dimensionality of graphene [11–13] and carbon nanotubes (CNTs) [13–17], the other two carbon allotropes. Meanwhile, there has been a recent paradigm shift toward the search of unusual high  $\kappa_l$  in some compounds made of both light and heavy elements with a large energy gap in the phonon

dispersion, such as semiconducting cubic phase boron arsenide (BAs) [18–22] and semimetallic  $\theta$ -phase tantalum nitride ( $\theta$ -TaN) [23,24].

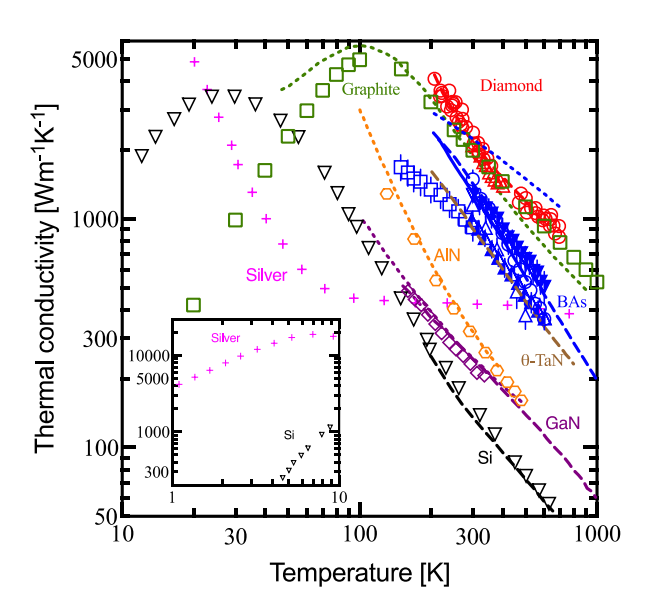


**Figure 1**: Comparison between theoretical (lines) and experimental (symbols) thermal conductivity data of diamond (red) [19,25,26], graphite (green) [27,28], BAs (blue) [18–22], θ-TaN (brown) [23], AlN (yellow) [29,30], GaN (purple) [31–33], Si (black) [19,34], and silver (pink) [35] with higher  $\kappa$  than most other common metals. The BAs experimental data include results from steady-state measurements (squares) [20] and time-domain thermal reflectance (TDTR) measurements (half-filled up-pointing triangles [21], unfilled up-pointing triangles [20], down-pointing triangles [22], and circles [36]). Naturally occurring isotope concentrations are considered in the theoretical results, for which four-phonon scattering is either neglected (dotted lines), treated with single mode relaxation time approximation (dashed lines), or calculated with an exact iterative numerical solution (solid lines). The calculation has assumed a length of 1 mm for graphite [27] and infinitely large crystals for the other materials. The inset shows the thermal conductivity of silver and Si in the temperature range from 1 to 10 K.

The common strategy for these different approaches to high  $\kappa_l$  is to minimize phonon scattering due to lattice anharmonicity, defects, boundaries, itinerary electrons, and spin fluctuation, the latter two of which are absent in non-magnetic dielectrics. While the defect densities and the grain size can be reduced and increased, respectively, to minimize their scattering of phonons, phonon-phonon scattering is an intrinsic property of the anharmonic lattice structure with nonlinear interatomic bonding. Identifying crystal structures with low phonon-phonon scattering rates is essential for the search of materials with an ultrahigh  $\kappa_l$ .

Recent progress in first-principles calculations of lattice dynamics combined with Boltzmann transport theory has considerably enhanced the capability for theoretical modeling of phonon-phonon scattering in different crystal structures [29,37]. This progress is highlighted by several recent successes. One of them is the prediction of ultrahigh  $\kappa_l$  in BAs with the inclusion of four-phonon scattering that goes beyond the lowest order of lattice anharmonicity responsible for three-phonon scattering processes [19,20]. Without four-phonon processes accounted for, another remarkable achievement is the prediction of phonon hydrodynamics in high- $\kappa_l$  graphitic materials at much higher temperatures than those observed previously in other bulk crystals [38,39]. Hydrodynamic phonon transport phenomena are analogous to momentum-conserving molecular scattering behaviors in gas flows and differ from heat diffusion processes underlying Fourier's law [40]. Supported by subsequent experiments of bulk BAs and graphite, these theoretical findings have advanced our understanding of phonon-phonon scattering processes and their impact on thermal transport.

As progresses are made to account for four-phonon scattering and phonon hydrodynamics in first principles calculations, new questions have emerged regarding whether four-phonon scattering is sufficient to weaken phonon hydrodynamics in two-dimensional (2D) graphene and

quasi one-dimensional (1D) CNTs and prevent them from breaking the  $\kappa_l$  records of diamond and graphite. These questions are related to the parallel study of length-divergent  $\kappa_l$  associated with the so-called super-diffusive lattice thermal transport behavior, which has been predicted for simplified low-dimensional systems since the celebrated work of Fermi, Pasta, Ulam, and Tsingou (FPUT) [41] in the 1950's. These questions are also relevant to the understanding of the conditions for observing ballistic phonon transport and quantized lattice thermal conductance in other 1D nanostructures [42–44] including a single-walled CNT (SWCNT) [45]. Addressing these questions are essential for advancing the fundamental understanding of quantized energy carrier transport beyond the established three-phonon scattering theory for not only these low-dimensional materials but also for bulk crystals with high  $\kappa$  and potentially non-diffusive behaviors of low-frequency modes [46].

These and other related outstanding questions are elaborated in the following sections. The discussion starts with a summary of the recent advance in theoretical computation of phonon scattering and  $\kappa_l$ , followed by a highlight of the theoretical and experimental studies of unusual high  $\kappa_l$  and four-phonon scattering in BAs. The roles of low-frequency modes and momentum-conserving normal scattering processes are then discussed in connection to length-divergent  $\kappa_l$  and phonon hydrodynamics, followed by an examination of the possible effects of four-phonon scattering on weakening phonon hydrodynamics and removing the length divergence in graphene and other low-dimensional systems. The effects of electron-phonon coupling, which can conserve the total momentum of the combined electron-phonon system and give rise to a drag effect on not only Seebeck coefficient but also mobility and  $\kappa_l$ , are described together with the prediction of high  $\kappa_l$  in semimetallic  $\theta$ -TaN compound. In the ballistic transport regime that is free of phonon-phonon and phonon-electron scattering, the challenges in experimental observation of the

quantized lattice thermal conductance phenomena in nanowires and nanotubes are discussed. Besides an emphasis on existing open problems in transport physics of ultrahigh- $\kappa$  materials, the last section of this perspective draws attention to emerging and untested approaches to breaking the diamond record in solid-state thermal transport. Instead of a comprehensive coverage of various recent works in the study of high- $\kappa$  materials, many of which have been discussed in some other recent reviews [47–49], this article has left out several important areas of recent research, especially the study of direct magnon and spinon contribution to  $\kappa$  [50,51] and their indirect effects on  $\kappa$  [52,53].

## Theoretical computation of phonon scattering and lattice thermal conductivity

Progress in theoretical computation of phonon-phonon scattering has played an enabling role in the discovery and understanding of ultrahigh- $\kappa_l$  materials. When the lattice potential energy (U) is expressed as a summation of polynomial functions of the atomic displacements, the third-order  $(U_3)$  and fourth-order  $(U_4)$  terms in this Taylor expansion represent the lowest order and second lowest order lattice anharmonicity. The atomic displacement can be expressed as a summation of the amplitudes  $(Q_\lambda)$ , which are associated with the number  $(n_\lambda)$  of phonons, of all the normal vibrational modes  $(\lambda)$  characterized by their respective wavevectors  $(\mathbf{q})$ , polarizations (p), angular frequency  $(\omega)$  [54,55]. The  $U_3$  perturbation term results in three-phonon scattering processes where two phonons are combined into a third phonon or a phonon splits into two other phonons. The  $U_4$  term yields four-phonon scattering processes, including two phonons merging into two other modes, one phonon splitting into three, and the reverse processes, as illustrated in Figure 2. The three- and four- phonon scattering processes conserve the total energy of lattice vibration  $(\Sigma_\lambda \ n_\lambda \hbar \omega)$  and alter the total crystal momentum  $(\Sigma_\lambda \ n_\lambda \hbar \mathbf{q})$  by an amount that vanishes

in normal scattering processes and equal a non-zero reciprocal lattice vector ( $\mathbf{G}$ ) in Umklapp processes. Here,  $\hbar$  is the reduced Planck constant.

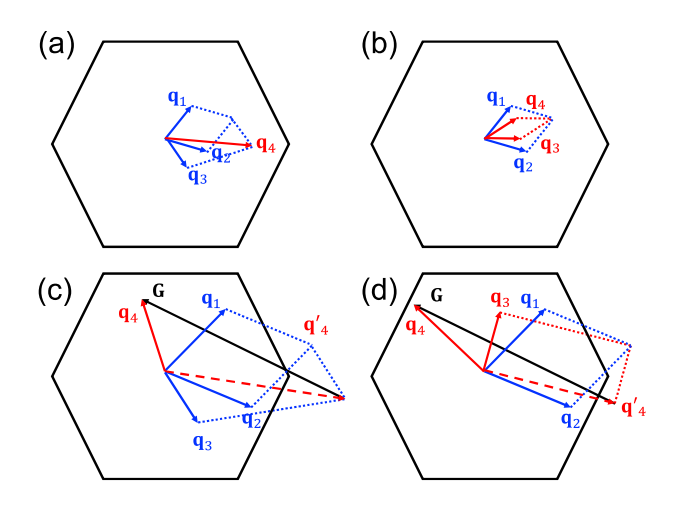


Figure 2: Diagrams of four-phonon scattering for normal (a,b) and Umklapp (c,d) processes, including (a)  $\mathbf{q}_1 + \mathbf{q}_2 + \mathbf{q}_3 = \mathbf{q}_4$ , (b)  $\mathbf{q}_1 + \mathbf{q}_2 = \mathbf{q}_3 + \mathbf{q}_4$ , (c)  $\mathbf{q}_1 + \mathbf{q}_2 + \mathbf{q}_3 + \mathbf{G} = \mathbf{q}_4$ , and (d)  $\mathbf{q}_1 + \mathbf{q}_2 + \mathbf{G} = \mathbf{q}_3 + \mathbf{q}_4$ .

Perturbation theory provides detailed expressions that use the anharmonic interatomic force constants (IFCs) to calculate the scattering rate term,  $\left(\frac{\partial n_{\lambda}}{\partial t}\right)_c$ , in the following steady-state Peierls-Boltzmann transport equation (PBTE) for phonons,

$$\boldsymbol{v}_{\lambda} \cdot \nabla T \frac{\partial n_{\lambda}}{\partial T} = \left(\frac{\partial n_{\lambda}}{\partial t}\right)_{C} \tag{1}$$

In this and the following equations, T is the temperature,  $v_{\lambda}$  and  $n_{\lambda}^{0} \equiv 1/\left[\exp\left(\frac{\hbar\omega_{\lambda}}{k_{\mathrm{B}}T}\right)-1\right]$  are the group velocity and the equilibrium Bose distribution of phonon mode  $\lambda$ , respectively, and  $k_{\mathrm{B}}$  is

the Boltzmann constant, respectively. With only linear terms in  $g_{\lambda} \equiv n_{\lambda} - n_{\lambda}^{0} \equiv -\frac{dn_{\lambda}^{0}}{dT} \nabla T \cdot \boldsymbol{F}_{\lambda}$  retained, the substituted PBTE can be simplified to [56]

$$F_{\lambda} = \tau_{\lambda}^{0} \left( \nu_{\lambda} + \Delta_{\lambda} \right) \tag{2}$$

Equivalent to a single-mode relaxation time (SMRT),  $\tau_{\lambda}^{0}$  due to contributions from three-  $(\tau_{\lambda}^{(3)})$  and four  $(\tau_{\lambda}^{(4)})$  phonon scattering processes is given by Matthiessen's rule as [20]

$$\frac{1}{\tau_{\lambda}^{0}} = \frac{1}{\tau_{\lambda}^{(3)}} + \frac{1}{\tau_{\lambda}^{(4)}} \tag{3}$$

Detailed expressions of  $\tau_{\lambda}^{(3)}$  and  $\tau_{\lambda}^{(4)}$  are given in the literature [20] as functions of  $n_{\lambda'}^0$  but not  $g_{\lambda'}$  or  $F_{\lambda'}$  of all the other modes ( $\lambda'$ ) that participate in three- and four-phonon processes with mode  $\lambda$ . As a correction to the SMRT approximation that does not account for the non-equilibrium distribution of other interacting modes [20],  $\Delta_{\lambda}$  is a function of  $F_{\lambda'}$  of all the other interacting modes ( $\lambda'$ ). The results are used to calculate

$$\kappa_{l} = -\frac{1}{V\nabla T} \sum_{\lambda} n_{\lambda} \hbar \omega_{\lambda} \boldsymbol{v}_{\lambda} = \int \tau_{\lambda}^{0} \left( v_{\lambda,\parallel} + \Delta_{\lambda,\parallel} \right) v_{\lambda,\parallel} \frac{dn_{\lambda}^{0}}{dT} \hbar \omega_{\lambda} \frac{d^{m}q}{(2\pi)^{m}}$$
(4)

where  $\|$  is used to denote the component antiparallel to  $\nabla T$ ,  $q \equiv |\mathbf{q}|$ ,  $d^m q \propto q^{m-1} dq$  is an infinitesimal volume of the m-dimension reciprocal space within the first Brillouin zone, V is the real space volume, and  $\frac{(2\pi)^m}{V}$  is the volume occupied by one  $\mathbf{q}$  state.

Accurate calculation of  $\tau_{\lambda}^{0}$  and  $\Delta_{\lambda}$  requires considerations of all processes that satisfy the momentum and energy conservation conditions in phonon-phonon scattering processes. Such computation was deemed "practically impossible" in the 1960's by Ziman due to the "the great complexity of the computation" [57]. Consequently, different SMRT approximation has been made. Among them, Callaway [58] estimated

$$\left(\frac{\partial n_{\lambda}}{\partial t}\right)_{C} \approx \frac{n_{\lambda}^{0} - n_{\lambda}}{\tau_{u}} + \frac{n_{\lambda}' - n_{\lambda}}{\tau_{n}} \tag{5}$$

In this model, Umklapp processes relaxes  $n_{\lambda}$  toward  $n_{\lambda}^{0}$  at a relaxation time  $(\tau_{u})$ , whereas momentum-conserving normal scattering processes relax  $n_{\lambda}$  toward the following displaced distribution with a non-zero drift velocity  $(\mathbf{u})$  at another relaxation time  $(\tau_{n})$ ,

$$n_{\lambda}' = \frac{1}{e^{\frac{\hbar(\omega - \mathbf{q} \cdot \mathbf{u})}{k_{\mathrm{B}}T}} - 1} \approx n_{\lambda}^{0} \left[ 1 + (n_{\lambda}^{0} + 1) \frac{\hbar \mathbf{q} \cdot \mathbf{u}}{k_{B}T} \right]$$
(6)

Under this assumption, the PBTE is simplified to

$$g_{\lambda} \approx -\left(1 + \frac{\beta}{\tau_n}\right) \tau_c v_{\lambda} \cdot \nabla T \frac{dn_{\lambda}^0}{dT}$$
 (7)

Here,  $\tau_c^{-1} \equiv \tau_u^{-1} + \tau_n^{-1}$ , and two different analytical expressions for  $\beta \equiv -\frac{\mathbf{q} \cdot \mathbf{u}}{\omega v_\lambda \cdot \frac{\nabla T}{T}}$  can be derived from the Debye approximation by considering that either the momentum change [58] or the rate of momentum change [59] vanishes upon normal scattering. Equivalent to taking  $\tau_\lambda^0 \approx \tau_c$  and  $\Delta_{\lambda,\parallel} \approx v_{\lambda,\parallel} \beta/\tau_n$ , the Callaway model uses adjustable parameters to calculate  $\tau_u$  and  $\tau_n$  without accounting for the actual scattering phase space.

Despite Ziman's statement that "The Boltzmann equation is so exceedingly complex that it seems hopeless to expect to generate a solution from it directly" [57], since 2007 Broido and coworkers [37] have advanced an iterative procedure [60,61] to solve for  $F_{\lambda}$  and  $\Delta_{\lambda}(F_{\lambda'})$  in Equation 2 for all the participating modes in the phase space without the use of any adjustable fitting parameters. This progress was built upon earlier density functional perturbative theory (DFPT) calculation of the third-order anharmonic IFCs of Si and Ge [62]. With the lowest order anharmonicity accounted for in the three-phonon scattering calculation of  $\Delta_{\lambda}$  and  $\tau_{\lambda}^{0}$ , the obtained  $\kappa_{l}$  is close to experimental values of diamond up to about 600 K and silicon up to about 300 K and higher than the experimental values at higher temperatures [19].

The discrepancy at high temperatures is expected to be caused by the neglect of higher order anharmonic terms in the interatomic potential than the third-order term responsible for three-

phonon scattering. Due to the large number of possible transitions that satisfy the selection rules, calculation of the four-phonon processes increases the computation cost tremendously compared to three-phonon scattering calculation. Nevertheless, Feng and Ruan were able to compute  $\tau_{\lambda}^{(4)}$  based on anharmonic lattice dynamical formalism of four-phonon scattering, a neglect of some infinitesimal IFCs, and additional approaches to mitigating the computational cost [63]. They further worked with Lindsay to include additional four-phonon scattering only in the calculation of  $\tau_{\lambda}^{(4)}$  but not in the iterative calculation of  $\Delta_{\lambda}$ , essentially assuming that four-phonon scatterings are all Umklapp processes [64]. With such approximation of four-phonon processes, the calculated  $\kappa_{l}$  decreases by 30% at 1000 K for both diamond and silicon and shows good agreement with the experimental results.

# Unusual high thermal conductivity and four-phonon scattering in BAs

Surprisingly, inclusion of the  $\tau_{\lambda}^{(4)}$  term in the calculation by Feng, Lindsay, and Ruan [64] considerably reduces the calculated room-temperature  $\kappa_l$  of BAs to 1400 W m<sup>-1</sup> K<sup>-1</sup> from 2330 W m<sup>-1</sup> K<sup>-1</sup>, which was previously calculated by Lindsay, Broido, and Reinecke with only three-phonon processes included in the iterative procedure [18]. Subsequently, a tetrahedron scheme was employed by Ravichandran and Broido to obtain convergence of the iterative solution of  $\Delta_{\lambda}(F_{\lambda'})$  with a modest grid size of the discretized Brillouin zone even when both three- and four-phono processes are included [20]. This approach results in a further reduction of the calculated room-temperature  $\kappa_l$  to 1260 W m<sup>-1</sup> K<sup>-1</sup> [20] for BAs with natural isotope abundances. It is worth noting that  $\beta$  and thus  $\Delta_{\lambda,\parallel}$  associated with normal scattering is expected to be a positive addition to  $v_{\lambda,\parallel}$  in Equation 4. Thus, the lower value calculated by the iterative procedure [20] than the earlier SMRT treatment of four-phonon processes [64] (see Figure 1) are associated with the

different IFCs and numerical schemes instead of the consideration of the normal scattering nature of some processes via the  $\Delta_{\lambda}(F_{\lambda'})$  term. With these differences removed, a latter SMRT treatment has indeed calculated an even lower  $\kappa_l$  value than the iterative procedure reported in the same work [20]. In any cases, even this reduced value is exceptionally high compared to the room-temperature values of only up to about 60, 140, 220, 300, 490, and 510 W m<sup>-1</sup> K<sup>-1</sup> for gallium arsenide (GaAs) [65], silicon (Si) [34], gallium nitride (GaN) [32], aluminum nitride (AlN) [30], boron phosphide (BP) [66], and silicon carbide (SiC) [67], respectively. In addition, isotope enrichment can increase these room temperature  $\kappa_l$  values by about 10% for both Si and BP [66], 5% for GaAs, 15% for GaN, and 50% for diamond, compared to 12% for BAs [68].

Compared to the thermal transport behaviors in this list of semiconductors, diamond, and graphite, both the high  $\kappa_l$  and pronounced four-phonon effect predicted in semiconducting BAs are unusual. For diamond and graphite, the ultrahigh  $\kappa_l$  originates from large phonon group velocities as a result of the low atomic mass and strong covalent bonding, low anharmonicity in the interatomic potential, and small scattering phase space due to the presence of only six phonon polarizations in this simple crystal structure with only two light carbon atoms occupying each lattice site. In contrast, BAs contains a light B and a heavy As atom at each lattice site. In such a binary compound, the upper frequency limit of the three acoustic phonon polarizations decreases with increasing mass of the heavy atoms that vibrate together with the adjacent light atoms, whereas the frequencies of the three optical phonon polarizations increase with decreasing mass of the light atoms that oscillate against the relatively stationary heavy atoms. The large atomic mass ratio between As and B produces a large energy gap between the acoustic (A) and optical (O) phonons, as shown in Figure 3(a). Due to the large A-O gap, combination of two acoustic phonons often cannot produce the energy of an optical phonon, forbidding such processes, as noted in

Ziman's analysis of interactions with optical modes [57] and some subsequent studies [69,70] of other III-V compounds over seven decades ago. In addition, the acoustic polarizations are bunched closely together in BAs. Based on Ziman's analysis of the selection rule [57], all possible scattering processes among three acoustic phonons would be wiped out in the extreme limit of three degenerate acoustic dispersions. Without being able to satisfy the energy and momentum selection rules, three-phonon scattering processes thus become rare in such compounds. In comparison, four-phonon processes, such as AAOO processes that involve two acoustic phonons and two optical phonons, become important in both BAs and some other III-V compounds that were found to exhibit a steeper T dependence of  $\kappa_l$  than the 1/T behavior associated with three-phonon processes [69,70]. Therefore, the peculiar features of the phonon band structure allow BAs to break conventional criteria and become the first known semiconductor with an ultrahigh  $\kappa_l$  where four-phonon scattering processes play an even more stronger role than other III-V compounds with much lower  $\kappa_l$ .

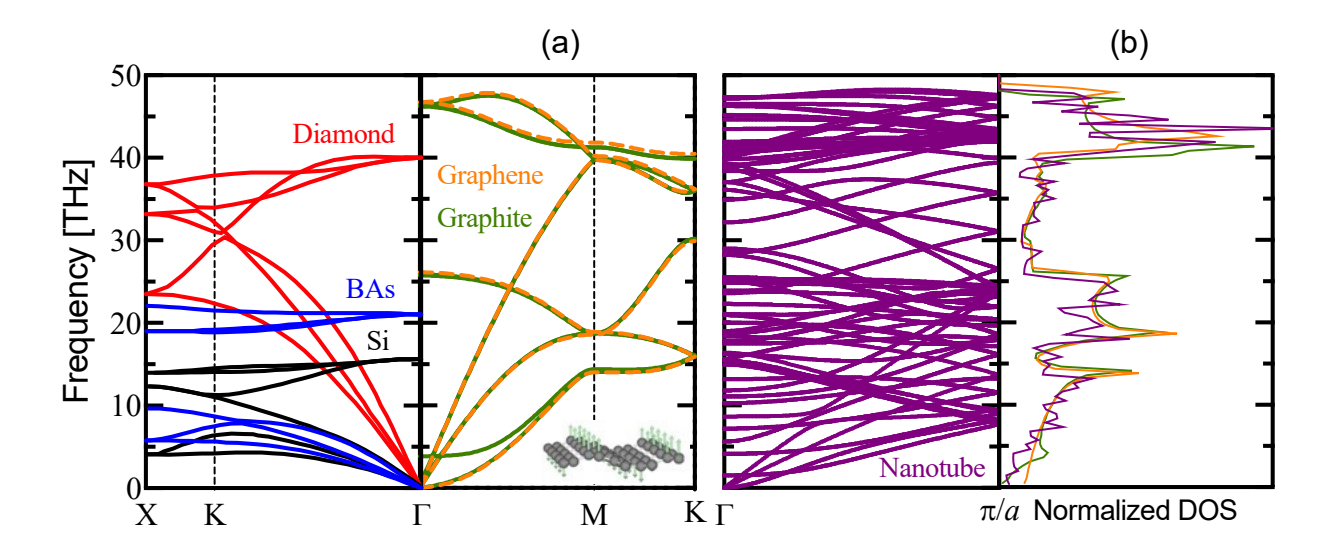


**Figure 3**: (a) Comparison of phonon dispersions of Si (black), BAs (blue), diamond (red), graphite (green), graphene (orange), and (10,0) SWCNT (purple). The inset illustrates the out-of-plane

atomic motion of the lowest-lying flexural (ZA) mode in graphene. In graphite, the lowest lying polarization is the gapless ZA polarization with a similar dispersion as the flexural polarization of graphene, whereas the ZO' polarization exhibits a gap of 3.87 THz at the zone center. In the nanotube, there are four gapless acoustic branches, including two doubly degenerate low-lying flexural branches, one torsional polarization, and one longitudinal polarization. (b) Phonon density of states (DOS) normalized by the number of atoms in the unit cell are for graphene (orange), graphite (green), and (10,0) SWCNT (purple).

Three separate experiments [20–22] have verified the predicted unusual high  $\kappa_l$  in BAs and a super-linear T dependence of  $1/\kappa_1$  associated with four-phonon processes, helping to turn initial skepticism of the first-principles four-phonon theory calculation into its acceptance. Moreover, another recent measurement [71] of the pressure-dependent  $\kappa$  of BAs has reported nearly perfect agreement with the theoretical prediction [72] of the competition between three-phonon and fourphonon processes at different pressures. As the crystal is under hydrostatic compressive strain, the phonon frequency is increased, especially for the optical modes and the longitudinal acoustic (LA) modes. Accordingly, the population decreases for the high-frequency optical phonons and largewavevector acoustic modes, which are required for Umklapp three-phonon scattering of propagating acoustic modes. For typical crystals,  $\kappa_l$  would increase with increasing pressure because of both an increase in the group velocity and a decrease in the Umklapp scattering rate of the propagating modes despite a decrease in the specific heat at low temperatures [57]. In particular, an increased pressure reduces the scattering rate for AAO processes involving two acoustic phonons and one optical phonon. For BAs with a large A-O gap, however, the AAO scattering rate is already low at ambient pressure, while the scattering rate for AAA processes involving three

acoustic phonons increases as the compressive strain separates the LA branch further from the two transverse acoustic (TA) polarizations. If only three-phonon scattering processes are accounted for, the  $\kappa_l$  of BAs and some other compounds with a large atomic ratio would decrease with increased pressure [73], opposite to the behaviors of other systems. When four-phonon scattering is considered, the  $\kappa_l$  of BAs contains a large contribution from phonons in the 4-8 THz range, where the scattering rate reaches a minimum for three-phonon processes and is maximized for the AAOO processes. The AAOO scattering rate decreases with increasing pressure due to an increase in frequency and decrease in population of optical phonons. Meanwhile, the scattering rate increases with pressure for AAA and AAAA scattering processes involving three and four acoustic phonons due to the increasing separation of LA phonons from TA phonons. As illustrated in Figure 4, the opposite pressure dependences of these three- and four- phonon scattering rates produce a non-monotonic pressure dependence of the BAs  $\kappa_l$  that peaks at an intermediate pressure, providing a compelling evidence of the unusual role of four-phonon processes in such a compound.

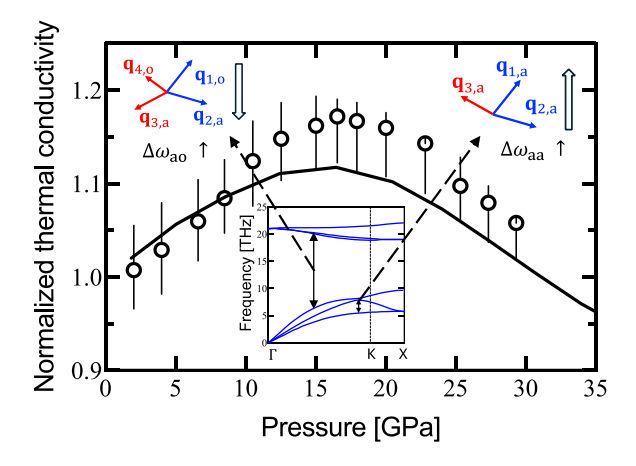


**Figure 4**: Anomalous pressure dependence of thermal conductivity of BAs from measurements (circles) [71] and theoretical calculations (solid curve) [72]. The pressure-dependent thermal conductivity is normalized by the value at ambient pressure. The inset illustrates that four-phonon

scattering is decreased and three-phonon scattering is increased with increasing pressure due to an increase of the A-O gap ( $\Delta\omega_{ao}$ ) and the LA-TA separation ( $\Delta\omega_{ao}$ ), respectively.

## Divergent thermal conductivity and the problem of long waves

Prior to the demonstration of ultrahigh- $\kappa_l$  BAs via the phonon band engineering paradigm, there have been various investigations of the possibility of realizing a divergent  $\kappa_l$  with increasing length of both bulk and low-dimensional systems below some characteristic temperatures for hydrodynamic and other non-diffusive phonon transport regimes. Referred as the problem of long longitudinal waves [57], k divergence with increasing length was previously suggested based on analyses [74,46] of the integral expression of  $\kappa_l$  of some bulk crystals. Even when the normal scattering correction term  $(\Delta_{\lambda,\parallel})$  is ignored, the  $\kappa_l$  integral in Eq. 4 would diverge if  $\tau_{\lambda}^0 \boldsymbol{v}_{\lambda,\parallel}^2$ increases with decreasing q at a rate not slower than  $q^{-m}$ , because  $n_{\lambda}^{0} \approx \frac{k_{B}T}{\hbar\omega_{\lambda}} >> 1$  and  $\frac{dn_{\lambda}^{0}}{dT}\hbar\omega_{\lambda}$  is approximately independent of  $\omega_{\lambda}$  or q for small-q and low- $\omega_{\lambda}$  modes. Each small-q phonon results in a lattice strain that is proportional to  $qQ_{\lambda}$ , whereas the mode amplitude  $Q_{\lambda}$  is proportional to  $\left(\frac{n_{\lambda}}{\omega_{\lambda}}\right)^{\frac{1}{2}}$  [55]. Depending on the strain energy, the net transition rate is proportional to  $qq'q''(n_{\lambda'}^0-n_{\lambda''}^0)$  and  $qq'q''(n_{\lambda'}^0+n_{\lambda''}^0+1)$ , respectively, for two types of scattering processes of three small-q acoustic phonons ( $\lambda, \lambda'$ , and  $\lambda$ ") that satisfy  $\omega_{\lambda} + \omega_{\lambda'} = \omega_{\lambda}$ " and  $\omega_{\lambda} = \omega_{\lambda'} + \omega_{\lambda'}$ " [46]. For the  $\omega_{\lambda} = \omega_{\lambda'} + \omega_{\lambda''}$  processes, q' and q'' are smaller than and approximately proportional to q,  $(n_{\lambda'}^0 + n_{\lambda''}^0 + 1)$  is proportional to  $q^{-1}$ , and the number of such processes scale as  $q^2$  for bulk crystals, resulting in a  $q^4$  dependence of the corresponding scattering rate  $(1/\tau_{\lambda}^{(3)})$ . For the  $\omega_{\lambda} + \omega_{\lambda'} = \omega_{\lambda''}$  processes, q' and q'' do not need to scale with q and can be

large,  $(n_{\lambda'}^0 - n_{\lambda''}^0)$  can be proportional to q, and degeneracy between two different phonon polarizations facilitates scattering of mode  $\lambda$  at the limit of vanishing q especially when it is not an LA mode, weakening the q dependence of  $1/\tau_{\lambda}^{(3)}$  compared to the  $q^4$  behavior. According to this analysis reported by Herring [46],  $\tau_{\lambda}^{(3)} v_{\lambda,\parallel}^2$  may still scale as  $q^{-4}$  or  $q^{-3}$  for the LA mode  $\lambda$  in some high-symmetry crystals without intercepting planes of degeneracy of phonon polarizations, potentially producing a divergent  $\kappa_l$  with increasing size of the crystal when four-phonon scattering is ignored.

Similar to the Landau–Rumer (L–R) microscopic damping model for sound waves [75], Herring's analysis [46] of the problem of long waves is focused on anharmonic interaction of a low-frequency sound phonon with two high-frequency thermal phonons that satisfy the momentum and energy conservations. These selection rules become invalid when the energy of the sound phonon with the angular frequency  $(\Omega)$  becomes comparable to the energy uncertainty of the thermal phonons, which is inversely proportional to their relaxation time ( $\tau_{th}$ ) [76]. Indeed, the lifetime calculated from a three-phonon scattering model has been found to be one order of magnitude larger than picosecond ultrasonic measurements of LA phonon attenuation in the 50-100 GHz frequency range [77]. In addition, TDTR measurements of the thickness-dependent  $\kappa$  of Si thin films have been used to extract smaller  $\kappa_l$  contributions from low-frequency phonons in bulk silicon than first-principles calculation of three-phonon scattering [78]. The discrepancy has been attributed [79] to macroscopic damping mechanisms of low-frequency sound phonons, including Akhiezer damping and thermoelastic damping [76,80], which are not accounted for in microscopic phonon scattering calculations. For ultrasounds with the angular frequency  $(\Omega)$  smaller than both  $1/\tau_{th}$  and  $k_BT/\hbar$ , the energy and wavelength of the sound wave are smaller and larger, respectively, than the energy uncertainty and wavelength of the thermal phonons. The

macroscopic strain field of the sound wave disturbs the wavevectors and occupation of packets of thermal phonons, which in return alter the speed of sound and relax the energy of the sound wave, resulting in the Akhiezer damping [76]. For  $\Omega < 1/\tau_{th}$ , Akhiezer damping weakens the frequency dependence of the relaxation time of the sound phonon compared to the Landau–Rumer model [77], further weakening or removing the  $\kappa_l$  divergence with increasing size for bulk crystals.

Compared to bulk crystals, a peculiar feature in the vibrational spectrum of a flat 2D system such as graphene is the behavior of the out-of-plane polarized flexural modes that propagate inside the basal plane. The Kirchhoff-Love classical plate theory [81] yields a quadratic dependence of the flexural mode frequency on its wavevector [82], see Figure 3(a), although coupling between the in-plane and bending strains tends to linearize the dispersion in the long-wavelength limit [83]. Moreover, Taylor expansion of either the lattice potential energy or electrostatic energy of the flat membrane does not yield product terms that consist of an odd number of out-of-plane atomic displacements, because flipping the out-of-plane displacement directions of all atoms does not alter the energy. This reflection symmetry prevents phonon-phonon scattering processes that involve an odd number of low-lying flexural phonons in a flat suspended 2D monolayer system [11]. This selection rule limits the three-phonon scattering phase space for flexural modes. Consequently, first-principles based calculation has found a large  $\kappa_l$  contribution from the flexural modes when only three-phonon scattering is accounted for [11]. As the reflection symmetry is broken to relax this selection rule in few-layer graphene, the three-phonon calculation obtains a decreased flexural mode contribution that reduces the basal-plane  $\kappa_l$  with increasing thickness from monolayer to bulk graphite.

The reflection symmetry does not prevent two flexural phonons with small wavevectors from being involved in a three-phonon scattering process. For the scattering of a linear mode  $\lambda$ 

with a pair of flexural phonons ( $\lambda'$  and  $\lambda''$ ) with a quadratic  $\omega_{\lambda} \propto q^2$  dispersion, the proportionality constant in the transition rate would become just q instead of qq'q''. For the scattering of a flexural phonon  $\lambda$  with another flexural phonon ( $\lambda'$ ) and a linear mode ( $\lambda''$ ),  $v_{\lambda,\parallel}^2$  would scale as q. If the number of three-phonon processes scale as  $q^{\alpha}$ , in addition, the  $\alpha$  constant is not expected to exceed m for an m-dimension systems. These factors would not increase the possibility for  $\kappa_l$  divergence in 1D and 2D systems if the normal scattering correction term is ignored. Indeed, neglecting the  $\Delta_{\lambda}$  term associated with normal scattering in a SMRT-based calculation would not only lower the  $\kappa_l$  value but also produce a convergent  $\kappa_l$  with increasing length of graphene and nanotube [16].

However, including the  $\Delta_{\lambda}$  term associated with normal scattering give rise to a length divergence of the  $\kappa_l$  obtained by the iterative solution of the PBTE for both graphene and the SWCNT when four-phonon processes are not considered and isotope scattering is considered separately from phonon-phonon scattering [11,16,84]. For the case of suspended monolayer graphene, the quadratic dispersion of the low-lying flexural modes give rise to a large population of small-q flexural phonons with a finite density of states at vanishing q, see Figure 3b. The wavevector of the third phonon due to the combination of two small-q flexural phonons still lies within the first Brillouin zone that contains all the inequivalent wavevectors. With only momentum-conserving normal scattering processes present, the total crystal momentum of phonons can remain a nonzero value indefinitely to give rise to a persistent heat flow even without the presence of a temperature gradient, giving rise to an infinite  $\beta$  in Eq. 7. Defect and surface scatterings are absent at the atomically smooth defect-free surfaces of suspended monolayer graphene and SWCNT, for which only the reflection at the end boundaries can cause resistance to the heat flow carried by the small-q modes if they are not involved in Umklapp processes. Consequently,  $\kappa_l$  calculated from Eq. 4 would diverge when the size of a defect-free crystal

increases to remove any extrinsic phonon scattering by boundaries, impurities, different isotopes, and defects.

In reality, a phonon transport regime with only normal processes but not Umklapp processes has not been found, because combination of two small-q phonons can result in a third large-q phonon that can be subject to subsequent Umklapp processes with other phonons. Nevertheless, normal scattering is exceptionally strong for the large-population of small-q flexural phonons to provide a competing mechanism that favors a divergent  $\kappa_l$  in 1D and 2D systems. For a SWCNT, in particular, three-phonon scattering among acoustic modes are found to be all normal processes in achiral (n,0) SWCNTs with  $n \ge 4$  due to the selection rule for angular quantum number [16]. Consequently, a  $L^{1/2}$  divergence of the calculated  $\kappa_l$  is obtained for a SWCNT when only three-phonon scattering is included [85]. At a length of 10  $\mu$ m, the calculated room-temperature  $\kappa_l$  for monolayer suspended graphene [11] and a (10,0) SWCNT [16] respectively reaches 3435 and 2242 W m<sup>-1</sup> K<sup>-1</sup>.

Momentum-conserving normal scattering process is similar to elastic collisions among gas molecules in a convective flow. At an intermediate temperature window where most excited phonon modes possess small energies and q, normal scatterings dominate Umklapp processes to yield not only the length divergence but also other hydrodynamic phonon transport features, that are analogous to the Poiseuille flow of gas molecules in a pipe and propagation of a pressure excitation pulse as a molecule density wave that is the ordinary sound. In a phonon Poiseuille flow [86], a non-uniform heat flux profile emerges in in a rod with a lateral size larger than  $l_n$  but smaller than  $(l_n l_u)^{1/2}$  [87], where  $l_n$  and  $l_U$  are the mean free paths for normal and Umklapp processes. When the a heating pulse width is smaller and larger than the relaxation times for normal and Umklapp processes, respectively, the heat pulse can propagates as a phonon density (or

temperature) wave referred as a second sound [40]. These two phenomena can be expressed as the analytical solutions of the macroscopic viscous heat equations, which couple the temperature and drift-velocity fields of the phonon population and are reduced to the heat diffusion equation in the limit of vanishing drift velocity [88]. They can also be obtained from microscopic Monte Carlo simulations of the PBTE, as shown in Figure 5 for graphite. Because frequent normal scattering among phonons increases the distance that phonons can travel before reaching the lateral boundary, phonon Poiseuille flow can occur and lead to a more rapid increase of the thermal conductance with *T* than the behavior of the ballistic conductance [89].

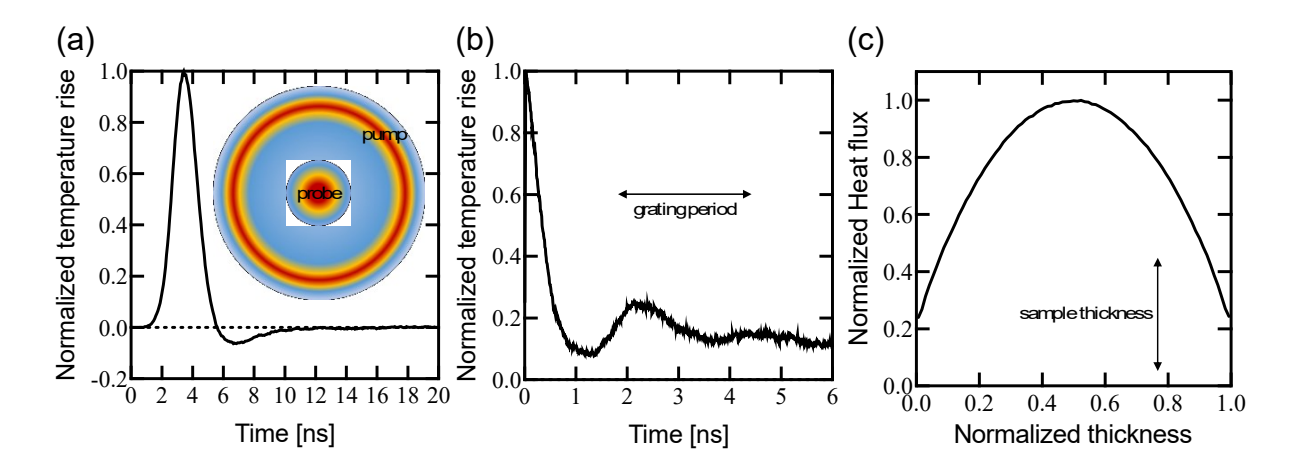


Figure 5: Monte Carlo simulations of phonon hydrodynamic phenomena in graphite. (a) Simulated temperature rise at the center probe beam location as a function of the delay time after the absorption of the ring-shaped pump pulse, showing transient lattice cooling effect near 7 ns delay time [90]. (b) Simulated temperature rise at the peak intensity location of the transient grating pattern of the pump beam as a function of the delay time after absorption of the pump pulse, showing wave-like temperature oscillation. (c) Simulated heat flux profile across the thickness direction of a 8.5 μm-thick graphite sample at 50 K, showing phonon Poiseuille flow [91]. The insets illustrate the corresponding top-down views of the sample schematic in the experiments. The ambient temperature is 80 K, 100 K, and 50 K for (a), (b), and (c), respectively.

Based on theories that consider only three-phonon scattering, these hydrodynamic phonon transport features would occur at a large temperature window approaching room temperature in graphene [38,39,89,92], graphite [90,91,93,94], and carbon nanotubes [95,96] due to frequent normal scattering of small-wavevector flexural modes. Second sound [90,93,94] and phonon Poiseuille flow[97] features have been observed in experiments with graphite at temperatures near 100 K and higher, which is one order of magnitude higher than those observed previously in other bulk materials such as sodium fluoride[98–101], solid helium[102,103], and bismuth[104]. This temperature increase is mostly caused by much more frequent normal scattering of low-frequency flexural phonons than Umklapp processes that involve zone-boundary modes at low occupations due to their high energies in the graphitic systems.

## Effects of four-phonon scattering in low-dimensional systems

Four-phonon scattering is known to weaken these non-diffusive transport behaviors. For four-phonon processes, the number of q' modes that can satisfy the selection rule increases and becomes relatively insensitive to q, preventing the divergence of the  $\kappa_l$  integral at sufficiently high temperatures where four-phonon processes become important in bulk crystals. Meanwhile, recent four-phonon calculations [84,105] of suspended monolayer graphene have suggested high four-phonon scattering rates for flexural modes due to the much larger density of states of these low-lying modes in graphene than in bulk graphite (see Figure 3), where interlayer interaction raises the energy of out-of-plane polarized modes by a gap that varies between zero for the ZA polarization to 3.87 THz for the ZO' mode where two adjacent graphene layers vibrate against each other. As the length of graphene is increased to above 10  $\mu$ m, the calculated room-temperature

basal-plane  $\kappa_l$  is still dominated by the flexural modes but only saturates to a value around 1300 Wm<sup>-1</sup>K<sup>-1</sup> [84], smaller than the 2000 W m<sup>-1</sup> K<sup>-1</sup> value reported from prior measurements of highly oriented pyrolytic graphite (HOPG) [28]. Compared to prior theories [11], this inclusion of four-phonon scattering [84] not only reverses the thickness dependence of the  $\kappa_l$  but also removes the  $\kappa_l$  divergence with increasing length at room temperature.

Besides this recent four-phonon calculation of graphene [84,105], another recent first principles-based study has shown that four-phonon scattering reduces the room-temperature  $\kappa_l$  of a (10,0) SWCNT to 4000 Wm<sup>-1</sup>K<sup>-1</sup> at room temperature [106], although further investigation of the convergence of the calculated  $\kappa_l$  with respect to the q mesh and sample length are required to better understand whether four-phonon scattering would also remove the length divergence of the room-temperature  $\kappa_l$  of the SWCNT. If four-phonon scattering can indeed suppress the  $\kappa_l$  of monolayer graphene [84,105] and SWCNT [106] considerably below the three-phonon limit according to these recent calculations, Umklapp scattering would play an more important role in the four-phonon processes than in the three-phonon process. This effect can likely lower the temperature window for the hydrodynamic regime than those calculated previously without three-phonon scattering [38,39,93,94].

There is still a lack of accepted  $\kappa_l$  value of suspended monolayer graphene due to the challenges in preparing high-quality suspended graphene samples and the lack of accurate measurement techniques. Meanwhile, the current capability in four-phonon calculations still cannot handle the case of graphite, for which experimental  $\kappa_l$  values are abundant and more accepted by the community than those on monolayer graphene. Therefore, the four-phonon calculation results for graphene still awaits experimental validation, while further four-phonon

calculations of few-layer graphene are needed to obtain insight into the  $\kappa_l$  dependence on the thickness of this system.

It is worth noting that length-divergent  $\kappa_l$  had been suggested by statistical thermodynamic analysis of non-linear lattice dynamics of simplified models of low-dimensional systems since the FPUT computation simulation of a 1D lattice chain [41]. The key finding from the FPUT simulation is that an initial vibrational mode in the 1D lattice chain cannot be thermalized with other modes to obtain an equilibrium distribution among the modes after a very long time. The original FPUT model has considered the  $U_4$  term associated with the second-order lattice anharmonicity but essentially accounts for only longitudinal vibrational modes along the lattice chain. Although recent works have considered transverse flexural modes with quadratic dispersion and observed length-divergent  $\kappa_l$  in low-dimensional systems [107–109], the lattice Hamiltonian models used in these calculations are highly simplified and do not consider the actual atomic structures of realistic 1D or 2D structures. Therefore, it is premature to use the findings from these 1D and 2D toy models to conclude that length divergence would occur for either a SWCNT or monolayer graphene at room temperature. Instead, the recent four-phonon calculation results for graphene give rise to a question whether higher order anharmonicity would lead to the convergent ki with length so that FPUT situation [41] would not occur in some of these realistic lowdimensional systems with large populations of low-frequency flexural modes that yield frequent four-phonon processes even at room temperature.

## Electron-phonon coupling in semiconductors and semimetals

Besides intriguing four-phonon scattering effects in high- $\kappa_l$  compounds and low-dimensional systems, electron-phonon coupling is another rich area of investigation for the search

of high- $\kappa_l$  metallic and semimetallic systems. In particular, electron-phonon coupling can have a pronounced effect on  $\kappa_l$  in binary compounds made of both heavy and light elements that produce a large A-O phonon gap to limit the phonon scattering rate. Compared to BAs, a number of these binary compounds such as niobium carbide (NbC) exhibit only moderate or low  $\kappa_l$  because phonons are scattered frequently by the large-density electrons in these metallic compounds [110]. The advance in first principles calculation of electron-phonon interactions [49,111] has recently enabled another theoretical proposal of an electron band engineering approach to high- $\kappa_l$  semimetallic binary compounds, such as  $\theta$ -TaN with a peculiar low electron density of states near the Fermi level to control electron-phonon scattering [23]. This theoretical proposal has motivated high-pressure synthesis of  $\theta$ -TaN crystals [24,112]. The measured room-temperature  $\kappa$  of initial polycrystalline θ-TaN samples is up to about 100 W m<sup>-1</sup> K<sup>-1</sup>, which is more than one order of magnitude higher than those reported for β-TaN<sub>x</sub> thin films commonly used as the diffusion barriers in interconnects [113]. As grain boundary scattering of phonons has limited the measured  $\kappa$  value to be a factor of 9 lower than the theoretical prediction for single-crystal  $\theta$ -TaN (see Figure 1), the theoretical proposal of electron-phonon band engineering approach to high- $\kappa_l$  semimetals remains a hypothesis that warrants future efforts in synthesis and characterization of  $\theta$ -TaN single crystals and other binary compounds, including a number of carbides and nitrides of group IV-V-VI transition metals, to illustrate the effects of electron density states on  $\kappa_l$ .

This initial proposal of electron-phonon band engineering approach [23] has yet to consider the momentum-conserving characteristics of electron-phonon coupling processes. Momentum conservation is not only essential in normal phonon-phonon and electron-electron scattering processes that are responsible for hydrodynamic transport of phonons [38,39,93] and electrons [114–116], respectively, but also relevant for electron-phonon coupling that controls  $\kappa_l$ , electron

mobility, and thermopower of semiconductors and semimetals. Momentum exchange between the phonon populations and electrons produce a drag contribution to these transport properties. The drag effect is a correction to the assumption of local equilibrium of the other type of energy carriers that interact with the one that is driven out of local equilibrium. For electrons driven out of local equilibrium by an electric field, the momentum exchange between electrons and phonons due to electron-phonon scattering yields a net phonon momentum along the same direction as the electron flux. Circulation of the net phonon momentum back to the electron system via electron-phonon coupling reduces the net electron momentum relaxation rate and increases the electron mobility [117] compared to the assumption of local equilibrium of the phonon bath. This effect also results in an additional phonon drag contribution to the Peltier coefficient and the Seebeck coefficient [118] besides the diffusion contribution that is calculated by assuming local equilibrium of the phonon bath. At low carrier densities, charge carriers with low kinetic energies are coupled mainly with low-frequency acoustic phonons, which are driven out of local equilibrium due to weak phonon-phonon scattering rate and become drag active. In BAs, phonon-phonon scattering rate is weak also for high-frequency acoustic modes, which become drag active and gives rise to a large phonon-drag thermopower calculated at a high hole concentration [119].

Conversely, when a temperature gradient is applied to drive a net electron flux toward the same direction as the net phonon flux, the calculated  $\kappa_l$  can be increased by considering the local non-equilibrium of the electron population compared to the case of assuming local equilibrium on the electrons. This latter electron drag effect of the  $\kappa_l$  has recently been calculated to be more pronounced in MoS<sub>2</sub> monolayer than in hexagonal AlN because the larger densities of states of low-energy electrons and phonons results in larger electron-phonon scattering phase space in the 2D semiconductor than in the 3D semiconductor [120]. It remains an open question whether this

electron-phonon drag effect may play an appreciable role in  $\theta$ -TaN and other semimetallic or doped compound semiconductors with low phonon-phonon scattering rates.

The recent predictions of electron-phonon coupling effects on the transport properties provide new directions for experimental studies of high- $\kappa$  materials. In several recent reports [71,121,122], inelastic X-ray scattering and vibrational electron energy loss spectroscopy (EELS) have been employed to probe phonon linewidths in high-k materials with different impurity doping or under different pressures. There are opportunities to employ these and other measurement techniques to investigate the phonon linewidth as a function of electric field doping to separate the effects of electron-phonon coupling on  $\kappa_l$  from those due to scattering by impurity doping. Initial efforts have been made to use an electric field to tune the charge carrier concentration in 2D graphene heterostructures during the thermal transport measurements to probe the direct electron contribution to  $\kappa_e$  and the indirect electron-phonon coupling effect on  $\kappa_l$  [123]. Further efforts are required to enhance the experimental capability to separate these two effects caused by electric field doping, as well as to distinguish the effects of phonon-impurity scattering and phononelectron coupling in  $\kappa_l$  of doped semiconductors and semimetals. Better understanding electronphonon coupling is essential for not only validating the electron-phonon band engineering approach to high- $\kappa_l$  semimetal [23], but is also relevant to experimental studies of the length dependence of thermal transport in graphene and CNT, where coupling between low-energy electrons and low-energy phonons may lead to drag and other effects on  $\kappa_l$ .

### Quantized lattice thermal conductance in nanowires and nanotubes

At the low-temperature limit, absence of internal scattering events leads to ballistic transport. When the roughness of the lateral surface of a rod is much smaller than the phonon

wavelengths, phonon scattering at the lateral surface is specular, conserve the longitudinal momentum, and does not contribute to thermal resistivity. In this case, resistive scattering only occurs at the end boundaries to increase the effective  $\kappa_l$  with increasing length in the ballistic regime. As the lateral dimension of a nanoscale conductor is further reduced to become comparable to the long wavelengths of low-frequency modes of the heat carrier, the allowable wavevectors are well separated along the lateral direction. A plot of the mode frequency dispersion as a function of the longitudinal wavevector ( $q_{\parallel}$ ) of an infinitely long 1D nanostructure would contain four gapless acoustic phonon polarizations (p) and additional optical polarizations with a gap at  $q_{\parallel}=0$ , as illustrated in Figure 3(a) for a (10, 0) SWCNT. For such a conductor with a length L connecting two thermal reservoirs at temperatures  $T^+$  and  $T^-$ , the ballistic lattice thermal conductance is given by the Landauer-Büttiker formalism as [42],

$$G_{b} = \frac{1}{(T^{+}-T^{-})L} \sum_{p} \sum_{v_{\lambda,\parallel}>0} \xi_{\lambda} \left[ n_{\lambda}^{0}(T^{+}) - n_{\lambda}^{0}(T^{-}) \right] \hbar \omega_{\lambda} v_{\lambda,\parallel} = \sum_{p} \int_{\omega_{\min,p}}^{\omega_{\max,p}} \xi_{\lambda} \frac{dn_{\lambda}^{0}}{dT} \hbar \omega_{\lambda} \frac{d\omega_{\lambda}}{2\pi}$$
(8)

If the transmission coefficient  $\xi_{\lambda}$  is unity for each of the four acoustic polarizations with  $\omega_{\min,p} = 0$  at infinite L, the thermal conductance contribution from each polarization at  $T \ll \hbar \omega_{\max,p}/k_{\rm B}$  would approach the quantized thermal conductance,

$$G_0 = \int_0^\infty \frac{dn_\lambda^0}{dT} \hbar \omega_\lambda \frac{d\omega_\lambda}{2\pi} = \pi k_B^2 T / 6\hbar$$
 (9)

Compared to the quantized electrical conductance that has been observed in measurements of nanoscale constrictions and point contacts at different temperatures [124–126], there have been few experimental attempts of measuring the quantized lattice thermal conductance. A pioneering experiment [43] found that the measured thermal conductance of four silicon nitride (SiN) beams, each with a 200 nm x 60 nm cross section, approached  $16G_{\theta}$  at temperatures below 0.8 K. The factor of 16 can be attributed to the presence of four beams each with four 1D acoustic

polarizations, including one longitudinal, one twisting, and two low-lying degenerate flexural polarizations with a quadratic dispersion. In comparison, a recent measurement [44] obtained much lower thermal conductance of SiN nanowires (NWs) than the quantized thermal conductance. Consequently, a recent review of modern physics [127] has called for more experiments to better demonstrate physics of 1D quantized lattice thermal transport.

The discrepancy between these few past experimental findings is due to the stringent conditions for observing quantized lattice thermal transport in the sub-Kevin temperature range. To avoid exciting the optical phonon modes such as the two low-lying transverse shear modes in a nanowire with a lateral dimension d, T needs to be much lower than  $T_c \approx \frac{2\pi\hbar v}{k_B d}$  so that optical modes with  $\omega_{\min,p} \gtrsim \frac{2\pi v}{d}$  would not be populated [128]. Above  $T_c$ , the thermal conductance is expected to transition to that of a three-dimensional system. Meanwhile, T needs to be larger than  $T_b \approx \frac{2\pi\hbar v}{k_B L}$  so that the dominant phonon frequency is above a cutoff set by the finite length as  $\omega^c \approx \frac{2\pi v}{k_B L}$ . Moreover, each of the two thermal reservoirs need to act as a uniform-temperature blackbody that emit phonons with an equilibrium Bose distribution at the reservoir temperature and absorb all incident phonons from the nanowire without reflecting them back into nanowire.

To minimize phonon reflection by the reservoir wall, in the past two experiments SiN membranes with 100 nm thickness (t) were patterned into suspended catenoidal nanowires with a width  $W(x) = W_n \cosh^2\left(\frac{x}{\lambda}\right)$  that increases with longitudinal distance (x) from the center as shown in the inset of Figure 6(a). Based on a recent Green's function calculation of phonon transmission,  $G_b$  approaches  $4G_0$  at T up to only 0.1 K and 0.2 K for the  $W_n$  value of 180 nm used in the earlier measurement [43] and the 100 nm value in the recent experiment [44], respectively, even when the  $\lambda$  value is taken as infinity. For the small  $\lambda$  value of 1  $\mu$ m used in the earlier measurement [43],

theoretical calculations have yet to be able to match the fine details of the measurement results, as shown in Figure 6(a). Meanwhile, the recent measurement results [44] are much lower than the Green's function calculation, leading to a hypothesis that phonons are scattered by other low-frequency excitations that causes a  $T^2$  instead of  $T^3$  dependence of its specific heat of the amorphous and defective structure at the low temperature limit. At the sub-K temperature range, moreover, the phonons exiting the nanowire into each of the two end reservoirs are likely not thermalized with the reservoir phonons effectively. Consequently, the thermometer placed at each end of the nanowire in the recent measurements [44] might have measured some average temperature of  $T^+$  and  $T^-$  instead of the required  $T^+$  and  $T^-$  value for the two opposite phonon flows in the nanowire.

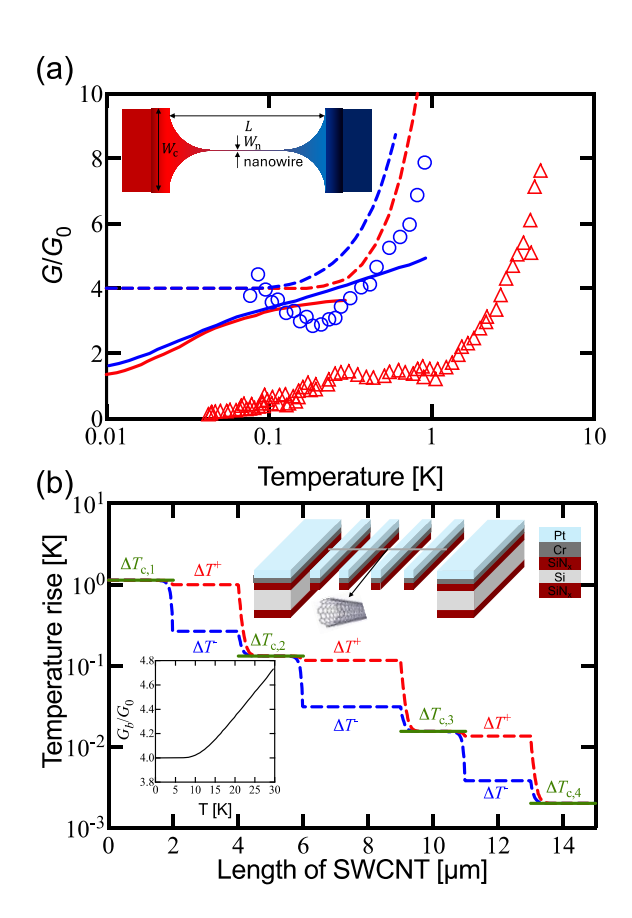


Figure 6: (a) Measurement and simulation data of quantized phonon conductance for catenary-shaped SiN nanowires illustrated in the inset, with  $L=4.4 \,\mu\text{m}$ ,  $W_c=4 \,\mu\text{m}$ ,  $W_n=180 \,\text{nm}$  for the data shown in blue and  $L=5 \,\mu\text{m}$ ,  $W=2.7 \,\mu\text{m}$ ,  $W_n=100 \,\text{nm}$  for the data shown in red in the main panel. The reported measurement results are shown as blue circles [43] and red triangles [44]. The solid curves show simulation results from atomic Green's function [129] (red) and lattice dynamics calculations [128] (blue). The dashed curves are the theoretical limit for L extended to infinity [129]. (b) Temperature profile schematic for ballistic phonon transport in a SWCNT suspended on a four-probe measurement device shown in the upper inset [130]. The green curve shows the thermometer temperature at the contact, while the red and blue curves represents the temperatures of left-moving and right-moving phonons in the nanotube. The lower inset shows the  $G_b/G_0$  ratio calculated in [45] for a semiconducting (10,0) SWCNT as a function of temperature.

Compared to amorphous SiN nanostructures measured previously, a defect-free SWCNT is free of two-level defects and surface roughness. Similar to SiN nanostructures, there are four gapless acoustic phonon polarizations in a SWCNT. The small diameters of SWCNTs lead to a large energy gap between the four acoustical polarizations and the other optical phonon branches. Thus, only the four acoustical phonon modes are populated in a relatively large temperature range, making it possible for only the four gapless acoustic modes to contribute to thermal transport at temperatures below about 10 K. Consequently, the calculated ballistic lattice thermal conductance  $(G_b)$  of a semiconducting (10,0) SWCNT approaches the quantized thermal conductance at a relatively high temperature up to about 10 K [45], as shown in the lower inset of Figure 6(b). However, it remains to be understood whether the large-population of low-frequency, small-q flexural modes in a SWCTN would be still subject to frequent normal scattering processes at that

temperature range, so that the ballistic transport regime would not be realized except for a very short SWCNT that cuts off the contribution from low-frequency phonons and raises  $\omega_{\min,p}$  to  $\omega^c \approx \frac{2\pi v}{L}$ .

Moreover, measurement of quantized lattice thermal conductance in SWCNTs is highly challenging because of the contact effects. Past thermal transport measurements have not obtained the intrinsic thermal conductance because the extrinsic interface thermal resistance has prevented the two-probe measurements from obtaining the intrinsic phonon conductance. These two-probe measurements have been based on electro-thermal microbridge platforms where one suspended SiN membrane was heated by an electric current in a serpentine platinum resistance thermometer patterned on the membrane, while the temperatures of this heating membrane and the adjacent sensing membrane were obtained from the measured electrical resistances of the corresponding resistance thermometers. A multi-probe thermal transport measurement has been reported to measure the contact thermal resistance and the thermal resistance of the suspended sample [131– 134]. More recently, a differential multi-probe method, illustrated in the upper inset of Figure 6(b), has been devised to completely eliminate the contact resistance error and obtain the  $\kappa_l$  of defective suspended multi-walled CNTs where phonon transport is in the diffusive regime [130]. A twotemperature model has also been proposed to analyze the multi-probe measurement result to obtain the intrinsic ballistic thermal conductance of a defect-free SWCNT when phonons are thermalized effectively at each contacted segments by interaction with the thermometer. Further detailed Green's function calculation of the interface transmission and thermalization processes is required to better understand whether this four-probe measurement can indeed allow for measurement of the ballistic and quantized lattice thermal conductance of a SWCNT.

## **Summary and outlook**

Much of the recent progress in high- $\kappa$  materials research has been driven by the establishment of a theoretical approach that combines first-principles calculation of lattice dynamics, quantum mechanical perturbation theory calculation of the phonon scattering rates, and iterative numerical solution of the Peierls-Boltzmann transport equation of phonons. Meanwhile, parallel progresses in first-principles calculation of electron-phonon scattering have not only allowed for the calculation of electron transport properties but also started to yield insights into the effects of electron-phonon coupling on lattice thermal transport [135]. Without requiring adjustable fitting parameters, this theoretical computation approach has elevated the predictive power in the search of high- $\kappa_l$  materials compared to prior phenomenological models, which were derived based on various approximations and used in the establishment of conventional criteria requiring simple crystal structures of strongly bonded light elements to achieve high  $\kappa_l$ . As a result, there has been a paradigm shift toward the search of high  $\kappa_l$  in compounds made of heavy and light elements.

Inclusion of four-phonon scattering processes in this theoretical computation approach has been a recent success and remained a frontier topic in the study of high- $\kappa$  materials. Before the recent four-phonon theory calculation result of graphene is validated by experiments, questions can still arise regarding whether the existing four-phonon calculations of BAs might have also underestimated its room-temperature  $\kappa$ . Currently, there is a lack of detailed characterization results on isotope impurities and other point defects in the existing BAs samples. Because it is usually very difficult to eliminate defects in the growth of binary compound crystals, it is intriguing that the measured thermal conductivity of BAs in one report [22] is already as high as the

theoretical maximum of the initial four-phonon SMRT calculation [64] and slightly higher than the subsequent full iterative solution with modest mesh sizes for BAs with natural isotope abundances [20]. Moreover, two TDTR measurements [20,36] have obtained steeper temperature dependence of the BAs thermal conductivity than existing four-phonon theory prediction. Questions have been raised on the use of diffusive Fourier's law to extract a single set of  $\kappa$  and thermal interface conductance values from the TDTR signals reflected by a thin film metal transducer deposited on BAs [136], where non-thermal distribution of phonons can be pronounced because the interface transmission coefficients and mean free paths are very large for low-frequency phonons compared to those for other modes. Moreover, the current phonon-phonon scattering formulism is derived from first-order perturbation theory, whereas a second order perturbation theoretical treatment of the three-phonon processes would produce another higher-order contribution in addition to the four-phonon term derived from the first-order perturbation theory [76]. Further theoretical and experimental studies are necessary to put these lingering questions to rest.

Advances in experimental studies of thermal transport in graphene, CNT, and other low-dimensional systems are essential for resolving the outstanding fundamental questions on four-phonon scattering of low-frequency modes. Progresses have been made to separate the contact resistance from the sample thermal resistance in resistive thermal resistance microbridge platform [131], and to identify the effects of local non-equilibrium [137] and strain [138] on micro-Raman thermometry measurements of low-dimensional nanostructures. Further innovations in measurements and analysis and sample preparation may enable multi-probe and other thermal transport measurements for studying non-diffusive, hydrodynamic, ballistic, and quantized

thermal transport in low-dimensional nanostructures to clarify whether these low-dimensional systems may exhibit divergent  $\kappa_l$  exceeding the diamond record.

Other unconventional approaches are essential for circumventing the difficulties in breaking the diamond record in solid-state thermal transport. As discussed in the preceding sections, the phono-phonon mean free paths, especially those for the Umklapp processes can be extremely long for low-frequency and long-wavelength modes, so that they flow through the materials with either few scattering or only momentum-conserving normal scattering events. Due to their low frequencies, their energy density is usually extremely low so that their thermal transport contribution can be large only when the materials size is extremely large to preserve their long mean free paths. Moreover, these low-frequency modes are often underpopulated in nanoelectronics and optoelectronics, where the electronic or optical excitations and the highfrequency optical phonons are coupled much more strongly with each other than with the lowfrequency phonon modes [86]. However, it is still possible to create an opposite type of nonthermal distributions with much larger energy density of these low-frequency modes than the Bose- Einstein distribution. One example of such a non-thermal distribution is the phonons transmitted across an interface that filter out high-frequency modes with low transmission coefficients [136]. In addition, short pulse heating has been used to produce acoustic pulses and coherent phonons [139], which are non-thermal distributions with the energy density highly concentrated in low-frequency modes. Some of these non-thermal distributions may allow enhanced thermal transport from the heat source, as suggested in a recent theoretical study [140].

These aforementioned open problems and potential new approaches to enhanced thermal transport are mostly within the framework of microscopic description of phonons and electrons as weakly interacting quasiparticles. Within this framework, the observed  $\kappa$  has yet to convincingly

exceed the diamond record that is actually dwarfed by the superconductivity in electrical transport. In superconductivity, a pair of electrons and a boson such as a phonon interact strongly to form a phase-coherent condensate below the critical temperature  $(T_c)$ . Such Cooper pairs are bosons that flow through materials without scattering. As the ground-state electron configuration, they do not carry entropy and thus do not contribute to  $\kappa$  directly. However, a Bose-Einstein condensate (BEC) may provide a completely different approach to high  $\kappa$ . One example is superfluid helium-4 ( ${}^{4}$ He) [141,142], which can an exhibit large effective  $\kappa$  that is proportional to  $\nabla T^{-2/3}$  [143,144] to be much larger than those of solids. At a temperature near  $T_c$ , the thermal transport behavior of  ${}^4\mathrm{He}$ has been described as a convective counterflow that is driven by the evaporation of the superfluid component (He II) into the normal fluid component (He I) at the hot side and the condensation of the normal fluid component into the superfluid component at the cold side, somewhat similar to the behavior of a heat pipe commonly used in electronic cooling. Periodic heating can produce a second sound as a wave propagation of the temperature or entropy field that depends on the ratio between the normal fluid and superfluid components. Due to the extremely low  $T_c$  of 2.17 K, superfluid <sup>4</sup>He has been used for cooling of only cryogenic instruments such as superconducting magnets. Several recent reports of high-temperature condensation signatures of magnons [145] and excitons [146-148] may stimulate new ideas of high-temperature solid-state analogues of helium-4 superfluid heat pipes [149] with extraordinary thermal transport performance.

#### References

- 1. A. L. Moore and L. Shi: Emerging challenges and materials for thermal management of electronics. *Materials Today* **17**(4), 163 (2014).
- 2. G. P. Thiel and A. K. Stark: To decarbonize industry, we must decarbonize heat. *Joule* **5**(3), 531 (2021).

- 3. Y. Muñoz-Maldonado, E. Correa-Quintana, and A. Ospino-Castro: Electrification of Industrial Processes as an Alternative to Replace Conventional Thermal Power Sources. *Energies* **16**(19), 6894 (2023).
- 4. Q. Zheng, M. Hao, R. Miao, J. Schaadt, and C. Dames: Advances in thermal conductivity for energy applications: a review. *Prog. Energy* **3**(1), 012002 (2021).
- 5. A. V. Sologubenko, E. Felder, K. Giannò, H. R. Ott, A. Vietkine, and A. Revcolevschi: Thermal conductivity and specific heat of the linear chain cuprate Sr 2 CuO 3: Evidence for thermal transport via spinons. *Phys. Rev. B* **62**(10), R6108 (2000).
- 6. C. Hess, C. Baumann, U. Ammerahl, B. Büchner, F. Heidrich-Meisner, W. Brenig, and A. Revcolevschi: Magnon heat transport in (Sr, Ca, La) 14 Cu 24 O 41. *Phys. Rev. B* **64**(18), 184305 (2001).
- 7. C. Hess, B. Büchner, U. Ammerahl, L. Colonescu, F. Heidrich-Meisner, W. Brenig, and A. Revcolevschi: Magnon Heat Transport in Doped L a 2 C u O 4. *Phys. Rev. Lett.* **90**(19), 197002 (2003).
- 8. C. Hess: Heat conduction in low-dimensional quantum magnets. *Eur. Phys. J. Spec. Top.* **151**(1), 73 (2007).
- 9. S. Guo, H. Li, X. Bai, Y. Wang, S. Li, R. E. Dunin-Borkowski, J. Zhou, and X. Chen: Size-dependent magnon thermal transport in a nanostructured quantum magnet. *Cell Reports Physical Science* **5**(3), 101879 (2024).
- 10. G. A. Slack: Nonmetallic crystals with high thermal conductivity. *Journal of Physics and Chemistry of Solids* **34**(2), 321 (1973).
- 11. L. Lindsay, D. A. Broido, and N. Mingo: Flexural phonons and thermal transport in graphene. *Phys. Rev. B* **82**(11), 115427 (2010).
- 12. J. H. Seol, I. Jo, A. L. Moore, L. Lindsay, Z. H. Aitken, M. T. Pettes, X. Li, Z. Yao, R. Huang, D. Broido, N. Mingo, R. S. Ruoff, and L. Shi: Two-Dimensional Phonon Transport in Supported Graphene. *Science* **328**(5975), 213 (2010).
- 13. A. A. Balandin: Thermal properties of graphene and nanostructured carbon materials. *Nature Mater* **10**(8), 569 (2011).
- 14. P. Kim, L. Shi, A. Majumdar, and P. L. McEuen: Thermal Transport Measurements of Individual Multiwalled Nanotubes. *Phys. Rev. Lett.* **87**(21), 215502 (2001).
- 15. E. Pop, D. Mann, Q. Wang, K. Goodson, and H. Dai: Thermal Conductance of an Individual Single-Wall Carbon Nanotube above Room Temperature. *Nano Lett.* **6**(1), 96 (2006).
- 16. L. Lindsay, D. A. Broido, and N. Mingo: Lattice thermal conductivity of single-walled carbon nanotubes: Beyond the relaxation time approximation and phonon-phonon scattering selection rules. *Phys. Rev. B* **80**(12), 125407 (2009).
- 17. L. Lindsay, D. A. Broido, and N. Mingo: Diameter dependence of carbon nanotube thermal conductivity and extension to the graphene limit. *Phys. Rev. B* **82**(16), 161402 (2010).
- 18. L. Lindsay, D. A. Broido, and T. L. Reinecke: First-Principles Determination of Ultrahigh Thermal Conductivity of Boron Arsenide: A Competitor for Diamond? *Phys. Rev. Lett.* **111**(2), 025901 (2013).
- 19. T. Feng, L. Lindsay, and X. Ruan: Four-phonon scattering significantly reduces intrinsic thermal conductivity of solids. *Phys. Rev. B* **96**(16), 161201 (2017).
- 20. F. Tian, B. Song, X. Chen, N. K. Ravichandran, Y. Lv, K. Chen, S. Sullivan, J. Kim, Y. Zhou, T.-H. Liu, M. Goni, Z. Ding, J. Sun, G. A. G. U. Gamage, H. Sun, H. Ziyaee, S. Huyan, L. Deng, J. Zhou, A. J. Schmidt, S. Chen, C.-W. Chu, P. Y. Huang, D. Broido, L.

- Shi, G. Chen, and Z. Ren: Unusual high thermal conductivity in boron arsenide bulk crystals. *Science* **361**(6402), 582 (2018).
- 21. S. Li, Q. Zheng, Y. Lv, X. Liu, X. Wang, P. Y. Huang, D. G. Cahill, and B. Lv: High thermal conductivity in cubic boron arsenide crystals. *Science* **361**(6402), 579 (2018).
- 22. J. S. Kang, M. Li, H. Wu, H. Nguyen, and Y. Hu: Experimental observation of high thermal conductivity in boron arsenide. *Science* **361**(6402), 575 (2018).
- 23. A. Kundu, X. Yang, J. Ma, T. Feng, J. Carrete, X. Ruan, G. K. H. Madsen, and W. Li: Ultrahigh Thermal Conductivity of θ -Phase Tantalum Nitride. *Phys. Rev. Lett.* **126**(11), 115901 (2021).
- 24. H. Lee, Y. Zhou, S. Jung, H. Li, Z. Cheng, J. He, J. Chen, P. Sokalski, A. Dolocan, R. Gearba-Dolocan, K. C. Matthews, F. Giustino, J. Zhou, and L. Shi: High-Pressure Synthesis and Thermal Conductivity of Semimetallic θ-Tantalum Nitride. *Advanced Functional Materials* **33**(17), 2212957 (2023).
- 25. J. Olson, R. Pohl, J. Vandersande, A. Zoltan, T. Anthony, and W. Banholzer: Thermal conductivity of diamond between 170 and 1200 K and the isotope effect. *Physical Review B* **47**(22), 14850 (1993).
- 26. D. G. Onn, A. Witek, Y. Z. Qiu, T. R. Anthony, and W. F. Banholzer: Some aspects of the thermal conductivity of isotopically enriched diamond single crystals. *Phys. Rev. Lett.* **68**(18), 2806 (1992).
- 27. G. Fugallo, A. Cepellotti, L. Paulatto, M. Lazzeri, N. Marzari, and F. Mauri: Thermal conductivity of graphene and graphite: collective excitations and mean free paths. *Nano letters* **14**(11), 6109 (2014).
- 28. A. De Combarieu: The Effects of Irradiation on the Thermal Conductivity at Low Temperatures of PseudoMonocrystalline Graphite. *Bull. Inst. Intern. Froid. Annexe* 2 63 (1965).
- 29. L. Lindsay, D. Broido, and T. Reinecke: Ab initio thermal transport in compound semiconductors. *Physical Review B* **87**(16), 165201 (2013).
- 30. Z. Cheng, Y. R. Koh, A. Mamun, J. Shi, T. Bai, K. Huynh, L. Yates, Z. Liu, R. Li, E. Lee, M. E. Liao, Y. Wang, H. M. Yu, M. Kushimoto, T. Luo, M. S. Goorsky, P. E. Hopkins, H. Amano, A. Khan, and S. Graham: Experimental observation of high intrinsic thermal conductivity of AlN. *Phys. Rev. Materials* **4**(4), 044602 (2020).
- 31. L. Lindsay, D. Broido, and T. Reinecke: Thermal conductivity and large isotope effect in GaN from first principles. *Physical review letters* **109**(9), 095901 (2012).
- 32. G. A. Slack, L. J. Schowalter, D. Morelli, and J. A. Freitas: Some effects of oxygen impurities on AlN and GaN. *Journal of Crystal Growth* **246**(3–4), 287 (2002).
- 33. N. K. Ravichandran and D. Broido: Phonon-Phonon Interactions in Strongly Bonded Solids: Selection Rules and Higher-Order Processes. *Phys. Rev. X* **10**(2), 021063 (2020).
- 34. C. J. Glassbrenner and G. A. Slack: Thermal Conductivity of Silicon and Germanium from 3°K to the Melting Point. *Phys. Rev.* **134**(4A), A1058 (1964).
- 35. C. Y. Ho, R. W. Powell, and P. E. Liley: Thermal Conductivity of the Elements. *Journal of Physical and Chemical Reference Data* **1**(2), 279 (1972).
- 36. S. Hou, F. Pan, X. Shi, Z. E. Nataj, F. Kargar, A. A. Balandin, D. G. Cahill, C. Li, Z. Ren, and R. B. Wilson: Ultrahigh Thermal Conductivity of Cubic Boron Arsenide with an Unexpectedly Strong Temperature Dependence. *arXiv*.2402.00248 (2024).

- 37. D. A. Broido, M. Malorny, G. Birner, N. Mingo, and D. A. Stewart: Intrinsic lattice thermal conductivity of semiconductors from first principles. *Applied Physics Letters* **91**(23), 231922 (2007).
- 38. S. Lee, D. Broido, K. Esfarjani, and G. Chen: Hydrodynamic phonon transport in suspended graphene. *Nat Commun* **6**(1), 6290 (2015).
- 39. A. Cepellotti, G. Fugallo, L. Paulatto, M. Lazzeri, F. Mauri, and N. Marzari: Phonon hydrodynamics in two-dimensional materials. *Nature Communications* **6**(1) (2015).
- 40. S. Lee and X. Li: in *Nanoscale Energy Transport*, edited by B. Liao (IOP Publishing, 2020), pp. 1-1-1–26.
- 41. E. Fermi, P. Pasta, S. Ulam, and M. Tsingou: Studies of the Nonlinear Problems (Los Alamos National Lab.(LANL), Los Alamos, NM (United States), 1955).
- 42. L. G. C. Rego and G. Kirczenow: Quantized Thermal Conductance of Dielectric Quantum Wires. *Phys. Rev. Lett.* **81**(1), 232 (1998).
- 43. K. Schwab, E. A. Henriksen, J. M. Worlock, and M. L. Roukes: Measurement of the quantum of thermal conductance. *Nature* **404**(6781), 974 (2000).
- 44. A. Tavakoli, K. Lulla, T. Crozes, N. Mingo, E. Collin, and O. Bourgeois: Heat conduction measurements in ballistic 1D phonon waveguides indicate breakdown of the thermal conductance quantization. *Nat Commun* **9**(1), 4287 (2018).
- 45. T. Yamamoto, S. Watanabe, and K. Watanabe: Universal Features of Quantized Thermal Conductance of Carbon Nanotubes. *Phys. Rev. Lett.* **92**(7), 075502 (2004).
- 46. C. Herring: Role of Low-Energy Phonons in Thermal Conduction. *Phys. Rev.* **95**(4), 954 (1954).
- 47. G. Chen: Non-Fourier phonon heat conduction at the microscale and nanoscale. *Nat Rev Phys* **3**(8), 555 (2021).
- 48. G. Benenti, D. Donadio, S. Lepri, and R. Livi: Non-Fourier heat transport in nanosystems. *Riv. Nuovo Cim.* **46**(3), 105 (2023).
- 49. F. Giustino: Electron-phonon interactions from first principles. *Rev. Mod. Phys.* **89**(1), 015003 (2017).
- 50. C. Hess: Heat transport of cuprate-based low-dimensional quantum magnets with strong exchange coupling. *Physics Reports* **811**, 1 (2019).
- 51. K. Vandaele, S. J. Watzman, B. Flebus, A. Prakash, Y. Zheng, S. R. Boona, and J. P. Heremans: Thermal spin transport and energy conversion. *Materials Today Physics* 1, 39 (2017).
- 52. M. Montagnese, M. Otter, X. Zotos, D. A. Fishman, N. Hlubek, O. Mityashkin, C. Hess, R. Saint-Martin, S. Singh, A. Revcolevschi, and P. H. M. Van Loosdrecht: Phonon-Magnon Interaction in Low Dimensional Quantum Magnets Observed by Dynamic Heat Transport Measurements. *Phys. Rev. Lett.* **110**(14), 147206 (2013).
- 53. D. A. Bozhko, V. I. Vasyuchka, A. V. Chumak, and A. A. Serga: Magnon-phonon interactions in magnon spintronics (Review article). *Low Temperature Physics* **46**(4), 383 (2020).
- 54. R. E. Peierls: Quantum Theory of Solids (Clarendon Press, 1955).
- 55. M. T. Dove: Introduction to Lattice Dynamics (Cambridge University Press, Cambridge, 1993).
- 56. W. Li, J. Carrete, N. A. Katcho, and N. Mingo: ShengBTE: A solver of the Boltzmann transport equation for phonons. *Computer Physics Communications* **185**(6), 1747 (2014).

- 57. J. M. Ziman: Electrons and Phonons: The Theory of Transport Phenomena in Solids (Oxford university press, 2001).
- 58. J. Callaway: Model for Lattice Thermal Conductivity at Low Temperatures. *Phys. Rev.* **113**(4), 1046 (1959).
- 59. P. B. Allen: Improved Callaway model for lattice thermal conductivity. *Phys. Rev. B* **88**(14), 144302 (2013).
- 60. M. Omini and A. Sparavigna: An iterative approach to the phonon Boltzmann equation in the theory of thermal conductivity. *Physica B: Condensed Matter* **212**(2), 101 (1995).
- 61. M. Omini and A. Sparavigna: Beyond the isotropic-model approximation in the theory of thermal conductivity. *Phys. Rev. B* **53**(14), 9064 (1996).
- 62. G. Deinzer, G. Birner, and D. Strauch: Ab initio calculation of the linewidth of various phonon modes in germanium and silicon. *Phys. Rev. B* **67**(14), 144304 (2003).
- 63. T. Feng and X. Ruan: Quantum mechanical prediction of four-phonon scattering rates and reduced thermal conductivity of solids. *Phys. Rev. B* **93**(4), 045202 (2016).
- 64. T. Feng, L. Lindsay, and X. Ruan: Four-phonon scattering significantly reduces intrinsic thermal conductivity of solids. *Phys. Rev. B* **96**(16), 161201 (2017).
- 65. R. O. Carlson, G. A. Slack, and S. J. Silverman: Thermal Conductivity of GaAs and GaAs1-x P x Laser Semiconductors. *Journal of Applied Physics* **36**(2), 505 (1965).
- 66. Q. Zheng, S. Li, C. Li, Y. Lv, X. Liu, P. Y. Huang, D. A. Broido, B. Lv, and D. G. Cahill: High Thermal Conductivity in Isotopically Enriched Cubic Boron Phosphide. *Adv Funct Materials* **28**(43), 1805116 (2018).
- 67. Z. Cheng, J. Liang, K. Kawamura, H. Zhou, H. Asamura, H. Uratani, J. Tiwari, S. Graham, Y. Ohno, Y. Nagai, T. Feng, N. Shigekawa, and D. G. Cahill: High thermal conductivity in wafer-scale cubic silicon carbide crystals. *Nat Commun* **13**(1), 7201 (2022).
- 68. K. Chen, B. Song, N. K. Ravichandran, Q. Zheng, X. Chen, H. Lee, H. Sun, S. Li, G. A. G. Udalamatta Gamage, F. Tian, Z. Ding, Q. Song, A. Rai, H. Wu, P. Koirala, A. J. Schmidt, K. Watanabe, B. Lv, Z. Ren, L. Shi, D. G. Cahill, T. Taniguchi, D. Broido, and G. Chen: Ultrahigh thermal conductivity in isotope-enriched cubic boron nitride. *Science* **367**(6477), 555 (2020).
- 69. E. F. Steigmeier and I. Kudman: Thermal Conductivity of III-V Compounds at High Temperatures. *Phys. Rev.* **132**(2), 508 (1963).
- 70. I. Kudman and E. F. Steigmeier: Thermal Conductivity and Seebeck Coefficient of InP. *Phys. Rev.* **133**(6A), A1665 (1964).
- 71. S. Li, Z. Qin, H. Wu, M. Li, M. Kunz, A. Alatas, A. Kavner, and Y. Hu: Anomalous thermal transport under high pressure in boron arsenide. *Nature* **612**(7940), 459 (2022).
- 72. N. K. Ravichandran and D. Broido: Non-monotonic pressure dependence of the thermal conductivity of boron arsenide. *Nat Commun* **10**(1), 827 (2019).
- 73. L. Lindsay, D. A. Broido, J. Carrete, N. Mingo, and T. L. Reinecke: Anomalous pressure dependence of thermal conductivities of large mass ratio compounds. *Phys. Rev. B* **91**(12), 121202 (2015).
- 74. I. Pomeranchuk: On the Thermal Conductivity of Dielectrics. *Phys. Rev.* **60**(11), 820 (1941).
- 75. L. Landau and G. Rumer: On the Absorption of Sounds in Solids. *Phys. Z. Sowjetunion* 11, 18187 (1937).
- 76. H. J. Maris: in *Physical Acoustics*, edited by W. P. Mason and R. N. Thurston (Academic Press, 1971), pp. 279–345.

- 77. B. C. Daly, K. Kang, Y. Wang, and D. G. Cahill: Picosecond ultrasonic measurements of attenuation of longitudinal acoustic phonons in silicon. *Phys. Rev. B* **80**(17), 174112 (2009).
- 78. P. Jiang, L. Lindsay, and Y. K. Koh: Role of low-energy phonons with mean-free-paths >0.8 µm in heat conduction in silicon. *Journal of Applied Physics* **119**(24), 245705 (2016).
- 79. A. A. Maznev: Onset of size effect in lattice thermal conductivity of thin films. *Journal of Applied Physics* **113**(11), 113511 (2013).
- 80. A. Akhiezer: On the Absorption of Sound in Solids. *Journal of Physics (Moscow)* **1**(1), 277 (1939).
- 81. A. E. H. Love: XVI. The small free vibrations and deformation of a thin elastic shell. *Phil. Trans. R. Soc. Lond. A* **179**, 491 (1888).
- 82. K. Komatsu and T. Nagamiya: Theory of the Specific Heat of Graphite. *J. Phys. Soc. Jpn.* **6**(6), 438 (1951).
- 83. K. Komatsu: Theory of the Specific Heat of Graphite II. J. Phys. Soc. Jpn. 10(5), 346 (1955).
- 84. Z. Han and X. Ruan: Thermal conductivity of monolayer graphene: Convergent and lower than diamond. *Phys. Rev. B* **108**(12), L121412 (2023).
- 85. N. Mingo and D. A. Broido: Length Dependence of Carbon Nanotube Thermal Conductivity and the "Problem of Long Waves." *Nano Lett.* **5**(7), 1221 (2005).
- 86. G. Chen: Nanoscale Energy Transport and Conversion: A Parallel Treatment of Electrons, Molecules, Phonons, and Photons (Oxford University Press, 2005).
- 87. D. G. Cahill and R. O. Pohl: Lattice Vibrations and Heat Transport in Crystals and Glasses. *Annu. Rev. Phys. Chem.* **39**(1), 93 (1988).
- 88. M. Simoncelli, N. Marzari, and A. Cepellotti: Generalization of Fourier's Law into Viscous Heat Equations. *Phys. Rev. X* **10**(1), 011019 (2020).
- 89. X. Li and S. Lee: Role of hydrodynamic viscosity on phonon transport in suspended graphene. *Phys. Rev. B* **97**(9), 094309 (2018).
- 90. J. Jeong, X. Li, S. Lee, L. Shi, and Y. Wang: Transient Hydrodynamic Lattice Cooling by Picosecond Laser Irradiation of Graphite. *PHYSICAL REVIEW LETTERS* **127**(8) (2021).
- 91. X. Li, H. Lee, E. Ou, S. Lee, and L. Shi: Reexamination of hydrodynamic phonon transport in thin graphite. *Journal of Applied Physics* **131**(7), 075104 (2022).
- 92. X. Li and S. Lee: Crossover of ballistic, hydrodynamic, and diffusive phonon transport in suspended graphene. *Phys. Rev. B* **99**(8), 085202 (2019).
- 93. S. Huberman, R. A. Duncan, K. Chen, B. Song, V. Chiloyan, Z. Ding, A. A. Maznev, G. Chen, and K. A. Nelson: Observation of second sound in graphite at temperatures above 100 K. *Science* eaav3548 (2019).
- 94. Z. Ding, K. Chen, B. Song, J. Shin, A. A. Maznev, K. A. Nelson, and G. Chen: Observation of second sound in graphite over 200 K. *Nat Commun* **13**(1), 285 (2022).
- 95. S. Lee and L. Lindsay: Hydrodynamic phonon drift and second sound in a (20,20) single-wall carbon nanotube. *Phys. Rev. B* **95**(18), 184304 (2017).
- 96. A. V. Savin and Y. S. Kivshar: Modeling of second sound in carbon nanostructures. *Phys. Rev. B* **105**(20), 205414 (2022).
- 97. X. Huang, Y. Guo, Y. Wu, S. Masubuchi, K. Watanabe, T. Taniguchi, Z. Zhang, S. Volz, T. Machida, and M. Nomura: Observation of phonon Poiseuille flow in isotopically purified graphite ribbons. *Nat Commun* **14**(1), 2044 (2023).

- 98. T. F. McNelly, S. J. Rogers, D. J. Channin, R. J. Rollefson, W. M. Goubau, G. E. Schmidt, J. A. Krumhansl, and R. O. Pohl: Heat Pulses in NaF: Onset of Second Sound. *PHYSICAL REVIEW LETTERS* **24**, 3 (1970).
- 99. H. E. Jackson and C. T. Walker: Thermal Conductivity, Second Sound, and Phonon-Phonon Interactions in NaF. *Phys. Rev. B* **3**(4), 1428 (1971).
- 100. D. W. Pohl and V. Irniger: Observation of Second Sound in NaF by Means of Light Scattering. *Physical Review Letters* **36**(9), 480 (1976).
- 101. H. E. Jackson, C. T. Walker, and T. F. McNelly: Second Sound in NaF. *PHYSICAL REVIEW LETTERS* **25**(1), 26 (n.d.).
- 102. L. P. Mezhov-Deglin: Measurement of the thermal conductivity of crystalline He4. *J. Exptl. Theoret. Phys.* **49**(1), 66 (1965).
- 103. C. C. Ackerman and W. C. Overton: Second Sound in Solid Helium-3. *Phys. Rev. Lett.* **22**(15), 764 (1969).
- 104. V. Narayanamurti and R. C. Dynes: Observation of Second Sound in Bismuth. *Physical Review Letters* **28**(22), 1461 (1972).
- 105. T. Feng and X. Ruan: Four-phonon scattering reduces intrinsic thermal conductivity of graphene and the contributions from flexural phonons. *Physical Review B* **97**(4) (2018).
- 106. A. Jain: Impact of four-phonon scattering on thermal transport in carbon nanotubes. *Phys. Rev. B* **109**(15), 155413 (2024).
- 107. J.-S. Wang and B. Li: Intriguing Heat Conduction of a Chain with Transverse Motions. *Phys. Rev. Lett.* **92**(7), 074302 (2004).
- 108. J.-S. Wang and B. Li: Mode-coupling theory and molecular dynamics simulation for heat conduction in a chain with transverse motions. *Phys. Rev. E* **70**(2), 021204 (2004).
- 109. S. Liu, X. F. Xu, R. G. Xie, G. Zhang, and B. W. Li: Anomalous heat conduction and anomalous diffusion in low dimensional nanoscale systems. *Eur. Phys. J. B* **85**(10), 337 (2012).
- 110. C. Li, N. K. Ravichandran, L. Lindsay, and D. Broido: Fermi Surface Nesting and Phonon Frequency Gap Drive Anomalous Thermal Transport. *Phys. Rev. Lett.* **121**(17), 175901 (2018).
- 111. S. Poncé, E. R. Margine, C. Verdi, and F. Giustino: EPW: Electron–phonon coupling, transport and superconducting properties using maximally localized Wannier functions. *Computer Physics Communications* **209**, 116 (2016).
- 112. Y. Liu, Q. Li, Y. Qian, Y. Yang, S. Wang, W. Li, and B. Sun: Thermal conductivity of high-temperature high-pressure synthesized θ-TaN. *Applied Physics Letters* **122**(22), 222201 (2023).
- 113. M. H. Tsai, S. C. Sun, H. T. Chiu, C. E. Tsai, and S. H. Chuang: Metalorganic chemical vapor deposition of tantalum nitride by tertbutylimidotris(diethylamido)tantalum for advanced metallization. *Applied Physics Letters* **67**(8), 1128 (1995).
- 114. D. A. Bandurin, I. Torre, R. K. Kumar, M. Ben Shalom, A. Tomadin, A. Principi, G. H. Auton, E. Khestanova, K. S. Novoselov, I. V. Grigorieva, L. A. Ponomarenko, A. K. Geim, and M. Polini: Negative local resistance caused by viscous electron backflow in graphene. *Science* **351**(6277), 1055 (2016).
- 115. J. Crossno, J. K. Shi, K. Wang, X. Liu, A. Harzheim, A. Lucas, S. Sachdev, P. Kim, T. Taniguchi, K. Watanabe, T. A. Ohki, and K. C. Fong: Observation of the Dirac fluid and the breakdown of the Wiedemann-Franz law in graphene. *Science* **351**, 6277 (2016).

- 116. R. Krishna Kumar, D. A. Bandurin, F. M. D. Pellegrino, Y. Cao, A. Principi, H. Guo, G. H. Auton, M. Ben Shalom, L. A. Ponomarenko, G. Falkovich, K. Watanabe, T. Taniguchi, I. V. Grigorieva, L. S. Levitov, M. Polini, and A. K. Geim: Superballistic flow of viscous electron fluid through graphene constrictions. *Nature Physics* 13(12), 1182 (2017).
- 117. Y. Quan, Y. Chen, and B. Liao: Significant phonon drag effect in wide band gap GaN and AlN. *Phys. Rev. B* **107**(24), 245202 (2023).
- 118. C. Herring: Theory of the Thermoelectric Power of Semiconductors. *Phys. Rev.* **96**(5), 1163 (1954).
- 119. C. Li, N. H. Protik, N. K. Ravichandran, and D. Broido: High-frequency phonons drive large phonon-drag thermopower in semiconductors at high carrier density. *Phys. Rev. B* **107**(8), L081202 (2023).
- 120. Y. Quan and B. Liao: Electron Drag Effect on Thermal Conductivity in Two-Dimensional Semiconductors. *Nano Lett.* **24**(26), 8143 (2024).
- 121. H. Uchiyama, T.-H. Liu, T. Ono, J. Fujise, B. Liao, S. Ju, G. Chen, and J. Shiomi: Quantifying doping-dependent electron-phonon scattering rates in silicon by inelastic x-ray scattering and first-principles lattice dynamics. *Phys. Rev. Mater.* **7**(10), 104601 (2023).
- 122. H.-H. Wu, H. Yang, C. A. Gadre, X. Yan, T. Aoki, B. Liao, Z. Ren, and X. Pan: Defect and Disorder Induced Phonon Softening in Boron Arsenide Using STEM-EELS. *Microscopy and Microanalysis* **29**(Supplement 1), 651 (2023).
- 123. M. M. Sadeghi, Y. Huang, C. Lian, F. Giustino, E. Tutuc, A. H. MacDonald, T. Taniguchi, K. Watanabe, and L. Shi: Tunable electron–flexural phonon interaction in graphene heterostructures. *Nature* **617**(7960), 282 (2023).
- 124. B. J. vanWees, H. vanHouten, Beenakker, Williamson, Kouwenhoven, D. vanderMarel, and Foxon: Quantized conductance of point contacts in a two-dimensional electron gas. *Physical review letters* **60**(9), 848 (1988).
- 125. S. Jezouin, F. D. Parmentier, A. Anthore, U. Gennser, A. Cavanna, Y. Jin, and F. Pierre: Quantum Limit of Heat Flow Across a Single Electronic Channel. *Science* **342**(6158), 601 (2013).
- 126. L. Cui, W. Jeong, S. Hur, M. Matt, J. C. Klöckner, F. Pauly, P. Nielaba, J. C. Cuevas, E. Meyhofer, and P. Reddy: Quantized thermal transport in single-atom junctions. *Science* **355**(6330), 1192 (2017).
- 127. J. P. Pekola and B. Karimi: *Colloquium*: Quantum heat transport in condensed matter systems. *Rev. Mod. Phys.* **93**(4), 041001 (2021).
- 128. Y. Tanaka, F. Yoshida, and S. Tamura: Lattice thermal conductance in nanowires at low temperatures: Breakdown and recovery of quantization. *Phys. Rev. B* **71**(20), 205308 (2005).
- 129. C. A. Polanco, A. Van Roekeghem, B. Brisuda, L. Saminadayar, O. Bourgeois, and N. Mingo: The phonon quantum of thermal conductance: Are simulations and measurements estimating the same quantity? *Sci. Adv.* **9**(41), eadi7439 (2023).
- 130. Q. Jia, Y. Zhou, X. Li, L. Lindsay, and L. Shi: Differential multi-probe thermal transport measurements of multi-walled carbon nanotubes grown by chemical vapor deposition. *International Journal of Heat and Mass Transfer* **216**, 124535 (2023).
- 131. J. Kim, E. Ou, D. P. Sellan, and L. Shi: A four-probe thermal transport measurement method for nanostructures. *Review of Scientific Instruments* **86**(4), 044901 (2015).

- 132. J. Kim, E. Fleming, Y. Zhou, and L. Shi: Comparison of four-probe thermal and thermoelectric transport measurements of thin films and nanostructures with microfabricated electro-thermal transducers. *J. Phys. D: Appl. Phys.* **51**(10), 103002 (2018).
- 133. E. Ou, X. Li, S. Lee, K. Watanabe, T. Taniguchi, and L. Shi: Four-Probe Measurement of Thermal Transport in Suspended Few-Layer Graphene With Polymer Residue. *Journal of Heat Transfer* **141**(6), 061601 (2019).
- 134. B. Smith, G. Fleming, K. D. Parrish, F. Wen, E. Fleming, K. Jarvis, E. Tutuc, A. J. H. McGaughey, and L. Shi: Mean Free Path Suppression of Low-Frequency Phonons in SiGe Nanowires. *Nano Lett.* **20**(11), 8384 (2020).
- 135. Y. Quan, S. Yue, and B. Liao: Impact of Electron-Phonon Interaction on Thermal Transport: A Review. *Nanoscale and Microscale Thermophysical Engineering* **25**(2), 73 (2021).
- 136. C. Hua, L. Lindsay, X. Chen, and A. J. Minnich: Generalized Fourier's law for nondiffusive thermal transport: Theory and experiment. *Phys. Rev. B* **100**(8), 085203 (2019).
- 137. S. Sullivan, A. Vallabhaneni, I. Kholmanov, X. Ruan, J. Murthy, and L. Shi: Optical Generation and Detection of Local Nonequilibrium Phonons in Suspended Graphene. *Nano Letters* **17**(3), 2049 (2017).
- 138. P. Sokalski, Z. Han, G. C. Fleming, B. Smith, S. E. Sullivan, R. Huang, X. Ruan, and L. Shi: Effects of hot phonons and thermal stress in micro-Raman spectra of molybdenum disulfide. *Appl. Phys. Lett.* **121**(18), 182202 (2022).
- 139. A. A. Maznev, F. Bencivenga, A. Cannizzo, F. Capotondi, R. Cucini, R. A. Duncan, T. Feurer, T. D. Frazer, L. Foglia, H.-M. Frey, H. Kapteyn, J. Knobloch, G. Knopp, C. Masciovecchio, R. Mincigrucci, G. Monaco, M. Murnane, I. Nikolov, E. Pedersoli, A. Simoncig, A. Vega-Flick, and K. A. Nelson: Generation of coherent phonons by coherent extreme ultraviolet radiation in a transient grating experiment. *Applied Physics Letters* 113(22), 221905 (2018).
- 140. V. Chiloyan, S. Huberman, A. A. Maznev, K. A. Nelson, and G. Chen: Thermal transport exceeding bulk heat conduction due to nonthermal micro/nanoscale phonon populations. *Applied Physics Letters* **116**(16), 163102 (2020).
- 141. L. Landau: Two-fluid model of liquid helium II. J. Phys. Ussr 5(1), 71 (1941).
- 142. R. P. Feynman: Atomic Theory of the Two-Fluid Model of Liquid Helium. *Phys. Rev.* **94**(2), 262 (1954).
- 143. J. H. Mellink: New measurements on the fountain effect and the heat conductivity of liquid helium II. *Physica* **13**(4), 180 (1947).
- 144. R. B. Dingle: Theories of helium II. Advances in Physics 1(2), 111 (1952).
- 145. D. A. Bozhko, A. A. Serga, P. Clausen, V. I. Vasyuchka, F. Heussner, G. A. Melkov, A. Pomyalov, V. S. L'vov, and B. Hillebrands: Supercurrent in a room-temperature Bose–Einstein magnon condensate. *Nature Phys* **12**(11), 1057 (2016).
- 146. Z. Wang, D. A. Rhodes, K. Watanabe, T. Taniguchi, J. C. Hone, J. Shan, and K. F. Mak: Evidence of high-temperature exciton condensation in two-dimensional atomic double layers. *Nature* **574**(7776), 76 (2019).
- 147. P. X. Nguyen, L. Ma, R. Chaturvedi, K. Watanabe, T. Taniguchi, J. Shan, and K. F. Mak: (2023).
- 148. R. Qi, A. Y. Joe, Z. Zhang, J. Xie, Q. Feng, Z. Lu, Z. Wang, T. Taniguchi, K. Watanabe, S. Tongay, and F. Wang: (2023).
- 149. P. Gully: Superfluid Helium Heat Pipe. Physics Procedia 67, 625 (2015).

#### **Authors contributions**

Both authors contributed to the writing of this manuscript.

# Acknowledgments

The authors thank Xiulin Ruan and Zherui Han for helpful discussions on four-phonon scattering and for providing the nanotube phonon dispersion data. The authors would also like to thank David Cahill and Ramamoorthy Ramesh for providing insightful comments on this manuscript. This work is a tribute to Natalio Mingo who lighted the journeys of many in this field over the past three decades.

## **Funding**

The authors' past and current works on BAs are supported by the Multidisciplinary University Research Initiative (MURI) of US Office of Naval Research (ONR Award No. N00014-16-1-2436) and the Future of Semiconductor Program of National Science Foundation (NSF) (Award No. 2329107), respectively. The studies of four-phonon processes in graphene and quantized thermal conductance in nanotubes are supported by NSF Thermal Transport Processes Program (Award No. 2321302) and Condensed Matter Physics Program (Award No. 2231376), respectively. The investigation of electronic switching of thermal transport is supported by ONR MURI (Award No. N00014-21-1-2377).

#### Data availability

All data generated or analyzed during this study are included in this published article.

#### **Conflict of interest**

The authors declare no conflict of interest.